FORMATION CONTROL OF AUTONOMOUS VEHICLES: DESIGN AND EXPERIMENTAL EVALUATION

A THESIS SUBMITTED TO
THE GRADUATE SCHOOL OF NATURAL AND APPLIED SCIENCES
OF
MIDDLE EAST TECHNICAL UNIVERSITY

BY

UĞUR MERTCAN ÖZMARANGOZ

IN PARTIAL FULFILLMENT OF THE REQUIREMENTS
FOR
THE DEGREE OF MASTER OF SCIENCE
IN
ELECTRICAL AND ELECTRONICS ENGINEERING

SEPTEMBER 2021

Approval of the thesis:

FORMATION CONTROL OF AUTONOMOUS VEHICLES: DESIGN AND EXPERIMENTAL EVALUATION

submitted by **UĞUR MERTCAN ÖZMARANGOZ** in partial fulfillment of the requirements for the degree of **Master of Science in Electrical and Electronics Engineering Department, Middle East Technical University** by,

Prof. Dr. Halil Kalıpçılar
Dean, Graduate School of **Natural and Applied Sciences** ______________

Prof. Dr. İlkay Ulusoy
Head of Department, **Electrical and Electronics Engineering** ______________

Prof. Dr. Klaus Werner Schmidt
Supervisor, **Electrical and Electronics Engineering, METU** ______________

Examining Committee Members:

Assoc. Prof. Dr. Emre Özkan
Electrical and Electronics Engineering, METU ______________

Prof. Dr. Klaus Werner Schmidt
Electrical and Electronics Engineering, METU ______________

Assist. Prof. Dr. Mustafa Mert Ankaralı
Electrical and Electronics Engineering, METU ______________

Assoc. Prof. Dr. Selahattin Çağlar Başlamışlı
Mechanical Engineering, Hacettepe University ______________

Assist. Prof. Dr. Halit Ergezer
Mechatronics Engineering, Çankaya University ______________

Date: 07.09.2021

I hereby declare that all information in this document has been obtained and presented in accordance with academic rules and ethical conduct. I also declare that, as required by these rules and conduct, I have fully cited and referenced all material and results that are not original to this work.

Name, Surname: Uğur Mertcan Özmarangoz

Signature :

ABSTRACT

FORMATION CONTROL OF AUTONOMOUS VEHICLES: DESIGN AND EXPERIMENTAL EVALUATION

Özmarangoz, Uğur Mertcan
M.S., Department of Electrical and Electronics Engineering
Supervisor: Prof. Dr. Klaus Werner Schmidt

September 2021, 81 pages

Research on fully-autonomous vehicles is a rising trend in the 21st century, since it is a promising area in which developments will be able to reduce work load of humans. As a specific research problem, studies on formation control theory have been done in the most recent years for fleets of autonomous vehicles in order to transform the way of transporting goods and individuals. This study focuses on a nonlinear virtual vehicle based controller, which is one of the formation control strategies in the literature. Since the existing work uses a kinematic vehicle model, this thesis extends the existing work to a dynamic bicycle car model, which is more realistic. Specifically, instead of assuming that the longitudinal and angular vehicle velocity can be directly applied as control inputs, the thesis designs controllers in order to track desired longitudinal and angular velocities provided by the formation controller. In a simulation study, the thesis compares the results of the kinematic and dynamic vehicle model, concluding that the formation control is satisfactory for the dynamic model if the designed controllers are tuned properly.

Keywords: Formation Controller, Virtual Structure Approach, Dynamic Bicylce Car Model, Gain Scheduling

ÖZ

OTONOM ARAÇLAR İÇİN FORMASYON KONTROLÜ: TASARIM VE DENEYSEL DEĞERLENDİRME

Özmarangoz, Uğur Mertcan
Yüksek Lisans, Elektrik ve Elektronik Mühendisliği Bölümü
Tez Yöneticisi: Prof. Dr. Klaus Werner Schmidt

Eylül 2021 , 81 sayfa

Tam otonom araçlar üzerine yapılan araştırmalar, gelişmelerin insanların iş yükünü azaltabileceği umut verici bir alan olması nedeniyle 21. yüzyılda yükselen bir trenddir. Spesifik bir araştırma problemi olarak, malları ve bireyleri taşıma şeklini dönüştürmek için son yıllarda otonom araç filoları için formasyon kontrol teorisi üzerine çalışmalar yapılmıştır. Bu çalışma, literatürdeki formasyon kontrol stratejilerinden biri olan doğrusal olmayan sanal araç tabanlı bir kontrolöre odaklanmaktadır. Mevcut çalışma bir kinematik araç modeli kullandığından, bu tez mevcut çalışmayı daha gerçekçi olan dinamik bir bisiklet araba modeline genişletmektedir. Spesifik olarak, lineer ve açısal araç hızının kontrol girdileri olarak doğrudan uygulanabileceğini varsaymak yerine, tez, formasyon kontrolörü tarafından sağlanan lineer ve açısal hızları izlemek için kontrolörler tasarlar. Bir simülasyon çalışmasında, tez, kinematik ve dinamik araç modelinin sonuçlarını karşılaştırır ve tasarlanan kontrolörlerin uygun şekilde ayarlanması durumunda formasyon kontrolünün dinamik model için tatmin edici olduğu sonucuna varılır.

Anahtar Kelimeler: Formasyon Kontrolü, Sanal Yapı Yaklaşımı, Dinamik Bisiklet Araç Modeli, Kazanç Ayarlama

To my family...

ACKNOWLEDGMENTS

First of all, I would like to express my sincere feelings about my supervisor Klaus Werner Schmidt for his support and guidance on taking the right actions during my thesis period. I am thankful for having the opportunity under his supervision that lead me to complete my thesis successfully.

I feel fortunate for having innovative, talented colleagues at Aselsan Inc. that help to increase my engineering strength and gain perspectives on how to look at a problem to resolve. I would like to thank M. Burak Gürcan and Umut Gökkaya who always support me during thesis works.

I would like to acknowledge Aselsan Inc., which helps me create time for my work on thesis.

I reserved to final statements for my great family and life partner. I am grateful for their unconditional love and support. They always gave me the power to overcome the problems that I encountered in tough times.

TABLE OF CONTENTS

LIST OF TABLES

TABLES

LIST OF FIGURES

FIGURES

LIST OF ABBREVIATIONS

AV	Autonomous Vehicle
GPS	Global Positioning System
CAV	Connected Autonomous Vehicles
APF	Artificial Potential Field
MPC	Model Predictive Controller
VC	Virtual Car

CHAPTER 1

INTRODUCTION

Autonomous vehicles (AVs) are self-driving cars which use a combination of sensors such as lidar, GPS, radar, etc. to sense their environment. In the recent years, an increasing amount of research effort is spent to reach the fifth level of autonomy which is Full Driving Automation [4–7]. The majority of the development is aimed at independent autonomous cars that can detect their environment and control the car based on that perception with no driver interaction. Self-driving cars have different possible usage areas such that personal commuting, transportation of goods for long distances, shared robotaxis and vehicle platooning [8–10]. If it is regulated properly, the usage of autonomous vehicles in urban environments will most likely reduce mortality in motor vehicle crashes caused by human error [11]. A specific topic for the automation of vehicles in traffic is to implement a generalized version of vehicle platooning, i.e., formation control for a fleet of AVs which is the goal of this thesis.

The goal of formation control is to ensure that all vehicles in a formation are moving at the same pace while preserving a desired formation shape, as defined by an inter-vehicle spacing strategy [12, 13]. Forming a formation with autonomous vehicles necessitates the use of particular algorithms, controllers, and tactics that include longitudinal and lateral control. Furthermore, for formation control, communication between the vehicles and sensing environment are necessary. In the literature, there are different strategies used to achieve formation control of AVs. The mostly used ones are Leader-Follower, Behavior Based and Virtual Based approaches [14]. In the Leader-Follower approach, a vehicle among the fleet is assigned as the leader while others are assigned as followers. There are also some works using the Behavioral Based Approach, where each vehicle in a group shows different behaviors due to the gathered information. There also strategies using a virtual rigid structure constructed by CAVs which is controlled to follow a path to keep the structure.

In this thesis work, a formation control algorithm which is based on the virtual leader approach is used [3]. To develop a formation controller, a virtual leader and a virtual structure around the leader is constructed with AVs. A nonlinear control algorithm is designed by applying a virtual orientation input via the backstepping technique in order to calculate the path of each vehicle to get in the desired position in the formation structure. After obtaining the path, a path following problem for AVs has to be solved. The formation controller is shown to be stable using Lyapunov Stability Theory in [3].

As the main contribution of this thesis, a disadvantage of the nonlinear formation controller in [3] is addressed. The designed formation controller is using a kinematic vehicle model to calculate a path for each AV, assuming it follows the path perfectly with calculated linear and angular velocity. In this work, a dynamic bicycle car model with a nonlinear tire model is used in order to obtain more realistic results. Specifically, controllers are designed to compute the acceleration and steering input of this model from the longitudinal and angular velocity signals provided by the nonlinear formation controller. Based on the realistic vehicle model and additional practical limitations, it is confirmed in simulations that the formation controller is able to sustain the desired virtual shape.

In short, the main contributions of the thesis are summarized as follows:

- Analysis of the nonlinear formation controller in [3],
- Development of a control structure for computing the acceleration and steering inputs of the dynamic bicycle model from the signals provided by the nonlinear formation controller,
- Design of controllers for the longitudinal and angular velocity of the dynamic bicycle model,
- Comprehensive simulations experiments that confirm the desired operation of the designed formation controller.

This thesis is organized as follows. In the first chapter of this thesis, motivation and scope of the thesis are provided. In Chapter 2, background information for autonomous vehicles is presented. In addition, formation control and strategies used in order to achieve formation control mostly which are leader-follower, behavioral and virtual based controllers are explained. Finally, the formation controller based on the virtual approach is provided from the literature which is used in this thesis. In Chapter 3, the dynamic bicycle model is provided mathematically, which is required to test the virtual-based formation controller with a more realistic vehicle model than the kinematic model. In order to model the cornering force of the tires, the magic formula is introduced. Then, in order to move the vehicle according to the reference signals supplied by the nonlinear formation controller, linear and velocity controllers are designed using P-controllers which are implemented using the gain scheduling technique. Finally, the vehicle model with velocity controller is exchanged with the kinematic model in the formation control strategy which is summarized in the previous chapter. The control performance when using the kinematic model and dynamic model are compared and limitations of the formation controller are described based on the obtained results. In Chapter 4, the thesis is concluded by discussing the results and providing plans for future works.

CHAPTER 2

BACKGROUND

In this chapter background information about nonholonomic vehicles, formation control and its strategies and the nonlinear virtual based formation controller used in this thesis are given.

2.1 Nonholonomic 4-Wheeled Autonomous Vehicles

A constraint of a system should be expressible as in Equation (2.1) to be called holonomic [15], whereby $u_1, \ldots, u_n$ are the system coordinates and t is time.

$$f(u_1, u_2, ..., u_n, t) = 0 \tag{2.1}$$

In other words, a holonomic constraint only depends on the coordinates and time. Accordingly, a system can be defined as a holonomic system if all constraints of the system are holonomic. Specifically, the state of a holonomic system does not depend on the velocity (time derivative of position). As a result, path integrals of a holonomic system are independent of the trajectory or transition between states but only depend on the initial and final states of the system.

Constraints which cannot be expressed as in (2.1) are called nonholonomic constraints. Therefore, nonholonomic constraints are nonintegrable [16]. That is, a nonholonomic system's final state depends on the initial state and trajectory between them. In particular, motion between two different positions at an infinitesimally-small distance might not always be possible [17].

Nonholonomic vehicles are described as systems which are constrained by rolling restrictions that limit the potential motion directions. They are not able to move sideways directly, but only rotate by moving forwards and backwards [18]. Therefore, daily used automobiles, cars and car-like robots are classified as nonholonomic vehicles. A nonholonomic car model is further detailed in Chapter 3.

2.2 Formation Control of Autonomous Ground Vehicles

Formation control or vehicle platooning is a method of controlling a group of unmanned vehicles which are called connected autonomous vehicles (CAVs) to follow a predetermined path while preserving a specific spatial pattern. Formation control is the next step of using fully automated vehicles in daily life commuting, transportation of individuals and goods. Vehicle platooning is an important component of traffic control because it provides numerous advantages, including increased safety, fuel economy, travel time, and decreased road congestion [14].

Mainly three different approaches are adopted in formation control theory which can be seen in Figure 2.1 [14].

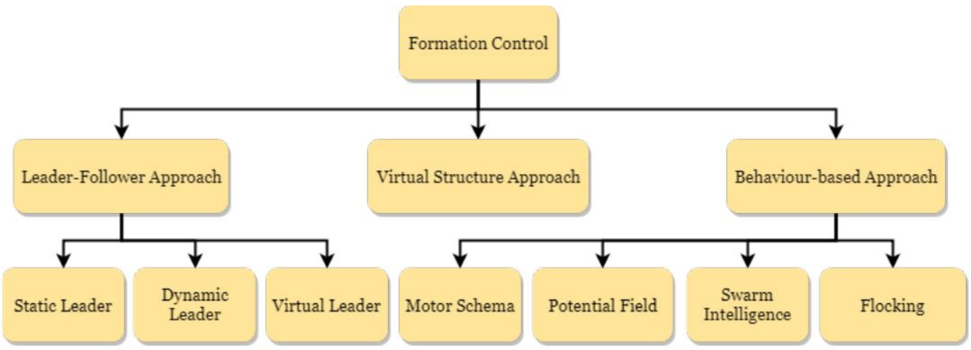

Figure 2.1: Formation Control Approaches

2.2.1 Leader-Follower Approach

The simplest solution to the formation control problem among three approaches is the leader-follower approach. In this technique, one of the robots in the fleet is assigned as leader of the formation and others are the followers. While the leader follows a predetermined path, the followers track the leader's position. The leader can be determined in three different ways: a static leader in which the leader robot remains the same throughout the formation control, a virtual leader who is employed by the program, and a dynamic leader, where the leader robot can change among the fleet in different situations [14].

The leader-follower method has the advantage of reducing tracking mistakes, and it can be analyzed using traditional control procedures. Furthermore, only the leader is responsible for trajectory planning, and others must follow the leader's path, resulting in a simpler controller. For inconvenience of this approach, a single mistake by the leader may penalize the entire formation. Also, data from the follower robots is not generally used as feedback for the leader's control loop in this method [19].

In order to give an example for leader-follower method from previously published research, in [20], to accomplish vehicle platooning for a bunch of nonholonomic robots, a gradient-based off-policy temporal-difference learning method was used. A static line follower is created in this study. A leader robot among the fleet traveled without the need for advanced path planning and the followers attempted to learn to follow the robot in front of them [21]. As longitudinal control of each follower vehicle, a neural dynamic programming method based on reinforcement learning was used. In this method, three layers of neural network is implemented for optimal throttle and break control policy. Inputs of the neural networks system are follower's speed and distance between itself and the vehicle in front and the output is the action of throttle or break depending on inputs.

In another publication [22], different controllers were implemented for the vehicle platooning of a fleet of AVs using leader-follower method. In order to achieve formation maintenance, feedback linearization controller was developed. An adaptive controller to cope with inaccurate relative distance of vehicles was used. Also, a robust adaptive controller was developed in order to decrease the effectiveness of external interference [23]. In order to confirm the stability of the cascaded system.

2.2.2 Behavior-Based Approach

In the behavior-based approach, each robot in a swarm has different behavior based on inputs from sensors such as avoiding obstacles, pursuing destination, and keeping formation [14]. Each behavior has a weight of significance and a coordinator chooses what the individual must do due to the information gathered from the sensors and importance level of the behavior. A network is structured between the robots in order to plan interacting behaviors. The final action of each robot is derived by the coordinator. The basic features of the behavior-based approach are listed below [24]:

- Behaviors are implemented by control rules,
- Inputs from the vehicle's sensors and modules in the system can be used for each behavior. Due to the effect of each behavior, actuators of robots can be commanded,
- Behaviors can get information from each sensor independently and command same actuators,
- Behaviours are defined as basic as possible, and they are gradually introduced to the system,
- Behaviors are executed simultaneously.

Since behaviors are executed through the information received from the sensors and other modules in the system, the most important advantage of this approach is that it can operate in unknown and dynamic environments. Furthermore, it is a parallel, on the spot and distributed method which is required less exchanging information [19]. On the other hand, group dynamics should be derived mathematically. It is also hard to obtain convergence and guarantee the stability of the whole formation [25].

In Figure 2.1, it can be seen that motor schema is a technique used for behavior-based approach. Motor schemas are action orders that achieve a goal-oriented behavior in agents. Schemas and motion primitives reflect a higher-level abstraction of robot activities, such as avoiding obstacles, avoiding robot, and keeping formation, rather than the simplest fundamental actions accessible to the AV, such as a single instruction to an actuator [26]. In a study [27], several motor schemas such as move-to-goal, avoid-static obstacle, avoid-robot, and maintain-formation were used to evaluate a variety of formation forms. These schemas were used to execute an agent's general behavior of moving to a desired place while avoiding obstacles and colliding with other agents in the fleet while maintaining the formation.

In another study [28], a distributed layered formation control framework was created to lead the robots as a group in an unfamiliar area while avoiding impediments and robot collisions. A leader–follower strategy for formation control and a behavior-based approach for obstacle avoidance were adopted in this work, and dynamic leader role switching was presented.

Another method for the Behavior-based approach is artificial potential field (APF) method. In this method, the objective and barriers in search spaces produce two fields for AVs [14]. The repellent force field created by barriers and the attractive force field generated by goals are the two fields. Closer to the barriers or objective, these factors are more powerful, whereas farther away, they have less of an impact. To calculate the robots' motion, speed, and direction of movement while avoiding a collision, the resultant forces (the total force) of the fields on the robots are utilized.

APF has been shown to be a good obstacle avoidance algorithm and is used to solve the formation problem. In a research [29], an algorithm for formation control and obstacle avoidance was simulated utilizing second-order consensus control and a modified APF approach. In another study [30], for the cooperative merging manoeuvre, an APF method was used with a longitudinal control scheme. A single controller was able to execute several tasks in this investigation, including vehicle following, gap closure, obstacle avoidance, and platoon merging.

2.2.3 Virtual-Based Approach

In the virtual-based approach, or virtual structure approach, a virtual rigid structure is derived by the group of robots. Each robot's movement is controlled with the given structure. In other words, the trajectory of each robot is not predefined but it is calculated from the movement of the structure. The same controller which minimizes the error between the desired structure position and actual position of the corresponding robot runs for each AV [14].

The advantage of using this virtual structure method is that achieving the coordinated behavior is simple [19]. However, a fault in the center of calculations may mean failure for the whole formation system. Furthermore, serious load of computation and communication is centered in one location, which may decrease the performance of the overall platoon [31].

Further advantages of the virtual-based approach are listed below [32]:

- There is no need for a robot to be assigned as leader,
- Virtual rigid body shape can be changed without need of modification in the system,
- A precise control of agents can be achieved,
- Tolerance to failure of the system during a failure of AVs in maintaining the rigid structure is built inherently.

In [33], a virtual structure method was used to control a vehicle convoy problem which is established when many CAVs move together across multiple lanes in a preplanned pattern. Vehicle platooning is established by dividing the convoy control issue into two different control methods which are virtual structure controller to control shape of the fleet and vehicle controller to control each vehicle in the fleet. A nonlinear model predictive controller (MPC) was constructed for autonomous driving by merging lane-keeping and collision avoidance behaviors. Another paper [34] suggested an architecture for adaptive virtual structure formation control, which involved designing a controller for nonholonomic mobile agents to track time-varying formations. Two controllers were developed in this research: a tracking controller for achieving stable tracking control performance during transitions between two formation configurations, and a formation controller for generating online formation reference and causing AVs to converge to a given formation shape.

The flexible virtual structure technique was used to provide a stabilizing control mechanism that assured that the agents in formation did not collide and that the intended shape was maintained [35]. To conduct multi-agent movement in this study, three control laws were used: an attractive control law to ensure convergence to the desired shape, a formation keeping and inter-robot collision avoidance rule, and an obstacle avoidance law. Furthermore, a controller was created to solve formation control problem of multiple wheeled nonholonomic mobile agents by ensuring that the Lyapunov candidate's derivative is negative definite, indicating that the controller is resilient to disturbances [3].

2.3 Nonlinear Virtual Based Formation Controller

In [3], formation control problem is solved following virtual based approach. In the study, each robot behaves as a particle of the rigid body. From the virtual structure, each robot's desired position with respect to the virtual car is derived. In Figure 2.2, the kinematic model used in this study can be seen.

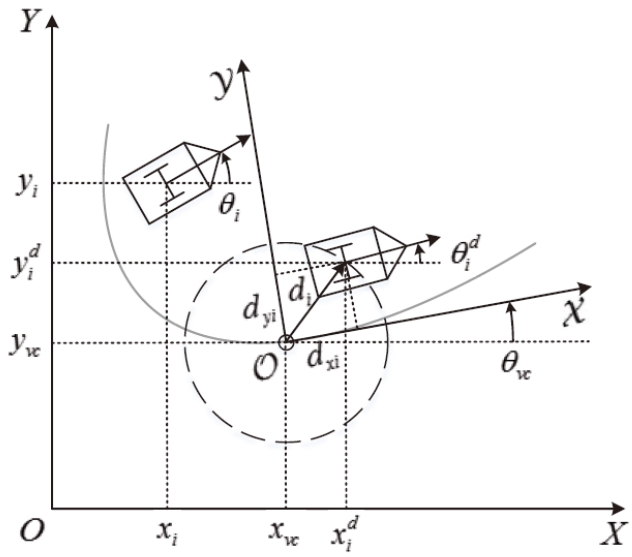

Figure 2.2: Kinematic Model of the Nonholonomic AV [3]

In the fleet of AVs, the i^{th} vehicle's kinematic model is formulated as below:

$$
\begin{aligned}
\dot{x}_i &= v_i \cos \theta_i \\
\dot{y}_i &= v_i \sin \theta_i \\
\dot{\Theta}_i &= w_i
\end{aligned}
\tag{2.2}
$$

Furthermore, the virtual controller's kinematic model is as follows:

$$\begin{aligned} \dot{x}_{vc} &= v_{vc} \cos \theta_{vc} \\ \dot{y}_{vc} &= v_{vc} \sin \theta_{vc} \\ \dot{\Theta}_{vc} &= w_{vc} \end{aligned} \tag{2.3}$$

There are two separate coordinate frames which are earth-fixed coordinate frame and virtual car fixed coordinate frame. The desired position of the i^{th} vehicle which is calculated from the desired shape of the rigid formation body is described as $[x_i^d \;\; y_i^d]$. The desired position of the vehicle in the virtual car fixed coordinate frame is described as $[d_{xi} \;\; d_{yi}]$. The desired position in the global coordinate is calculated as below:

$$\begin{aligned} x_i^d &= x_{vc} + d_{xi} \cos \theta_{vc} - d_{yi} \sin \theta_{vc} \\ y_i^d &= y_{vc} + d_{xi} \sin \theta_{vc} + d_{yi} \cos \theta_{vc} \end{aligned} \tag{2.4}$$

Then, the error can be defined as

$$\begin{aligned} e_{xi} &= x_i^d - x_i \\ e_{yi} &= y_i^d - y_i. \end{aligned} \tag{2.5}$$

In the study, the virtual controller is derived by applying a virtual orientation control input via using the backstepping technique. The resulting controller, which determines the linear velocity of the i^{th} vehicle, i.e. $[v_i \;\; w_i]$ where the vehicle is moving forward can be seen below:

$$v_i = \sqrt{\tilde{x}_i^2 + \tilde{y}_i^2}, \tag{2.6}$$

where

$$\begin{aligned} \tilde{x}_i &= \dot{x}_i^d + k_i \tanh(e_{xi}) \\ \tilde{y}_i &= \dot{y}_i^d + k_i \tanh(e_{yi}) \end{aligned} \tag{2.7}$$

The angular speed controller is derived as

$$w_i = \dot{\theta}_i^* + k_{\theta i} \bar{e}_{\theta i} \tag{2.8}$$

with the desired angular velocity

$$\dot{\theta}_i^* = \frac{-[\ddot{x}_i^d + k_i \mathrm{sech}^2(e_{xi}) \dot{e}_{xi}] \tilde{y}_i + [\ddot{y}_i^d + k_i \mathrm{sech}^2(e_{yi}) \dot{e}_{yi}] \tilde{x}_i}{v_i^2} \tag{2.9}$$

and the heading error

$$\bar{e}_{\theta i} = \theta_i^* - \theta_i, \tag{2.10}$$

which is computed from the actual heading θ_i and the desired heading θ_i^*:

$$\theta_i^* = \text{atan2}(\tilde{y}_i(0), \tilde{x}_i(0)) + \int_t \dot{\theta}_i^* \, dt \tag{2.11}$$

In Equation (2.7), k_i is a controller constant of the i^{th} vehicle in the fleet. Also, in Equation (2.8), $k_{\theta i}$ is the controller constant of the i^{th} vehicle in the fleet for angular speed. In [3], the effect of a change in k_i and $k_{\theta i}$ is not examined. These constants are decided as $k_i = 1$ and $k_{\theta i} = 3$ for each AV in the fleet.

In order to examine the effect of varying k_i and $k_{\theta i}$, a simulation is carried out, whose results can be seen in Figures 2.3, 2.4, 2.5 and 2.6. In this simulation, the virtual car is assumed to travel straight ($w_{vc} = 0$) with constant linear speed. Also in Table 2.1, the initial values and desired position of vehicle w.r.t. the virtual car can be seen. Firstly, the nonlinear formation controller is tested with 3 different k_i values ([0.5 1 5]) while $k_{\theta i}$ is constant ($k_{\theta i} = 3$). Then, k_i is left constant ($k_i = 1$) and the effect of $k_{\theta i}$ is tested with 3 different values ([1 3 9]).

Table 2.1: Control Parameters Test Initial Conditions

$v_{vc}[m/s]$	$w_{vc}[^o/s]$	$x_{des}[m]$	$y_{des}[m]$	$X_0[m]$	$Y_0[m]$
20	0	1	1	-3	3

In Figure 2.3, it can be seen that as k_i gets higher, the settling time of the formation controller gets lower. However, there occurs overshoot on the angular velocity of the vehicle in Figure 2.4. Furthermore, the lateral acceleration of the vehicle exceeds $3\,\text{m/s}^2$, which is undesirable for such vehicles. When $k_i = 1$, the lateral acceleration is within admissible limits. A similar result is true for varying $k_{\theta i}$ case which can be seen in Figures 2.5 and 2.6. For $k_{\theta i}$ above 3, the lateral acceleration of the vehicle exceeds the limit. Therefore, the same values for k_i and $k_{\theta i}$ as in [3] are used ($k_i = 1$ and $k_{\theta i} = 3$) in this thesis.

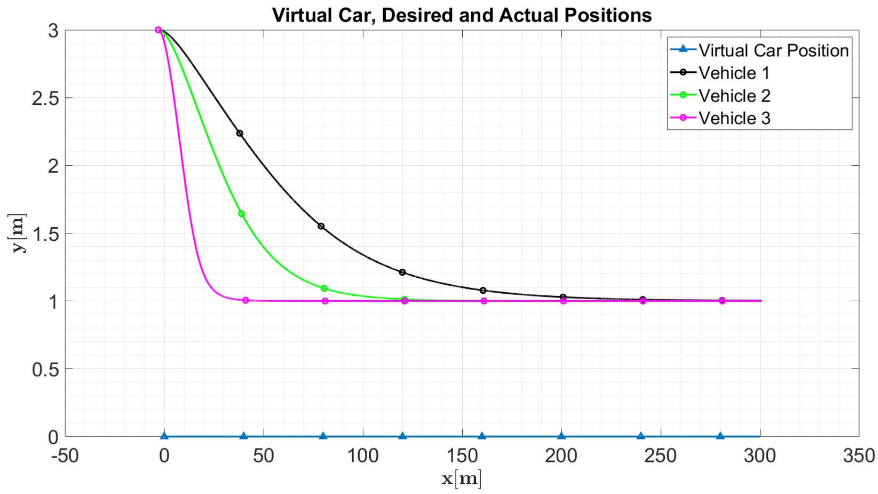

Figure 2.3: Vehicle Positions for $v_{vc} = 20\,\text{m/s}$, $k_{\theta i} = 3$, $k = [0.5\ 1\ 5]$

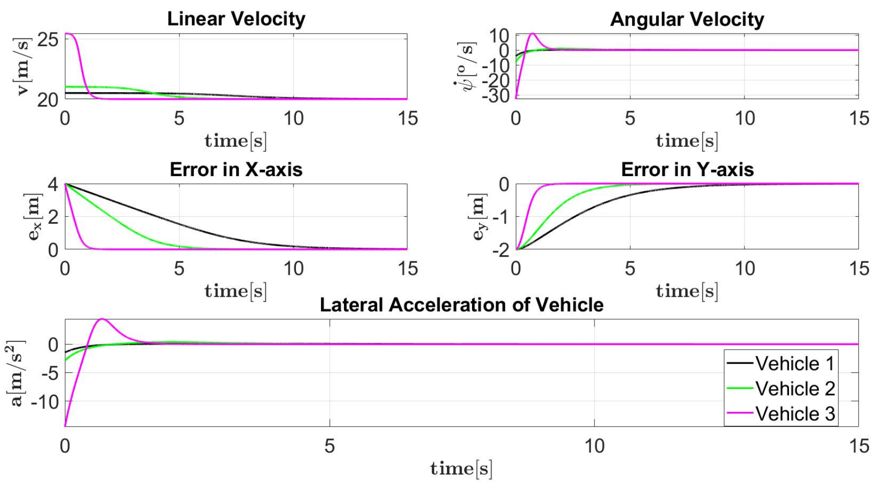

Figure 2.4: Linear and Angular Velocity, Error in X and Y Axis, Lateral Acceleration of Vehicle for $v_{vc} = 20\,\text{m/s}$, $k_{\theta i} = 3$, $k = [0.5\ 1\ 5]$

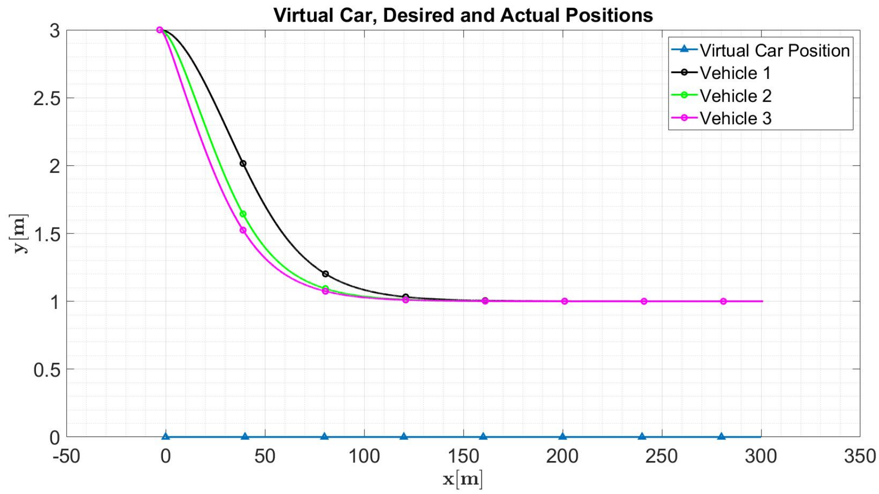

Figure 2.5: Vehicle Positions for $v_{vc} = 20\,\text{m/s}$, $k_{\theta i} = [1\;3\;9], k = 1$

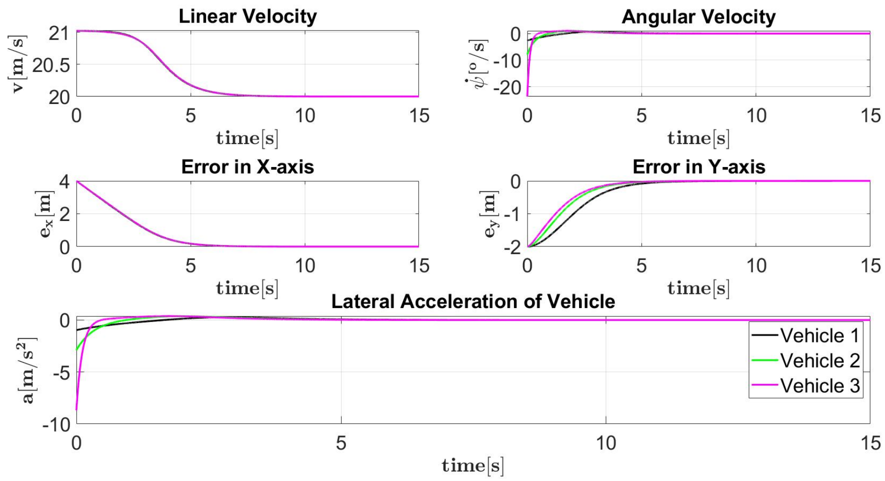

Figure 2.6: Linear and Angular Velocity, Error in X and Y Axis, Lateral Acceleration of Vehicle for $v_{vc} = 20\,\text{m/s}$, $k_{\theta i} = [1\;3\;9], k = 1$

Some additional simulation tests for the nonlinear formation controller in different cases can be seen below for illustration. In these tests, Tables 2.2, 2.3 and 2.4 show the desired position with respect to the virtual car position and the initial positions in the global coordinate frame. Figures 2.7, 2.10 and 2.13 show the linear velocity, angular velocity and lateral acceleration of the virtual car. Furthermore, the positions of the vehicles and virtual car throughout the simulation time is depicted in Figures 2.8, 2.11 and 2.14. Lastly, the linear and angular velocities, error in x and y directions and lateral acceleration of each car in the fleet are given respectively in Figures 2.9, 2.12 and 2.15.

2.3.1 Case 1

In the first test case, we consider that the virtual vehicle travels on a straight line with a constant velocity.

Table 2.2: Case 1: Desired and Initial Positions

x_1^{des}	y_1^{des}	x_2^{des}	y_2^{des}	x_3^{des}	y_3^{des}
-2	8	0	3	-2	-8
$X_1(0)$	$Y_1(0)$	$X_2(0)$	$Y_2(0)$	$X_3(0)$	$Y_3(0)$
-15	15	-12	-8	0	-25

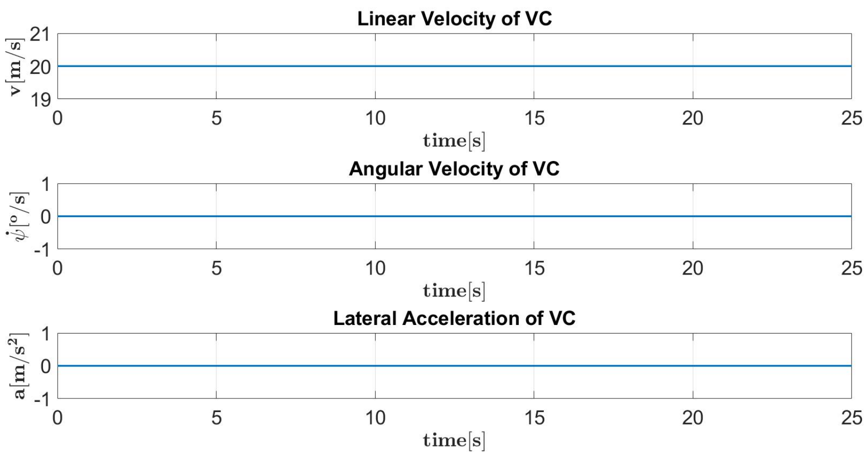

Figure 2.7: Case 1: Linear Velocity, Angular Velocity and Lateral Acceleration of Virtual Car

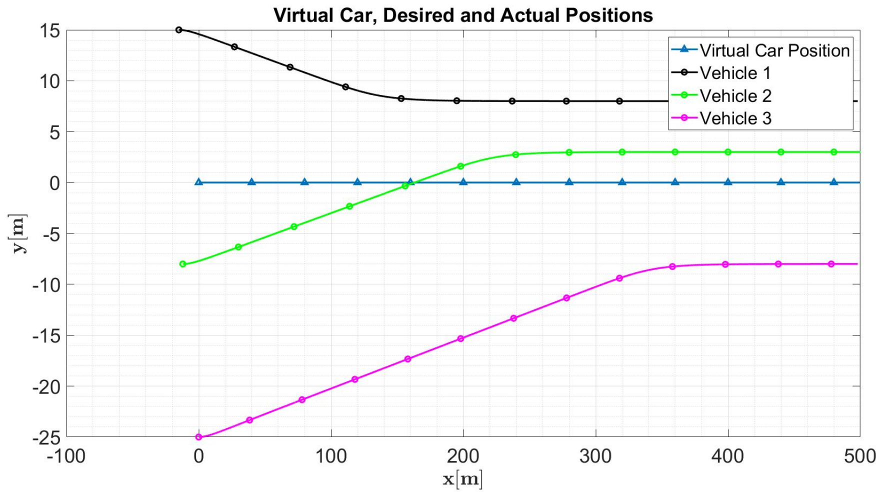

Figure 2.8: Case 1: Position of Vehicles and Virtual Car

It is readily observed from Figure 2.8 and 2.9 that, even all vehicles do not start on their desired trajectory, the vehicle trajectories converge to the desired formation by adjusting their longitudinal and angular velocities. Hereby, the lateral acceleration is initially high due to the deviation from the desired trajectory.

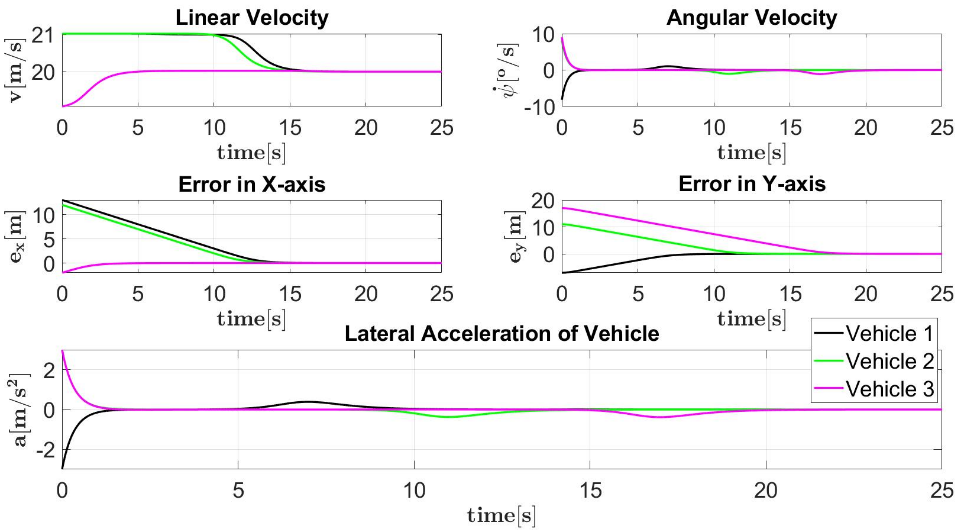

Figure 2.9: Case 1: Linear and Angular Velocity, Error in X and Y Direction and Lateral Acceleration of Vehicles

2.3.2 Case 2

In the second test case, we consider that the virtual vehicle travels on a circular path at a constant velocity.

Table 2.3: Case 2: Desired and Initial Positions

x_1^{des}	y_1^{des}	x_2^{des}	y_2^{des}	x_3^{des}	y_3^{des}
-6	6	6	0	-6	-6
$X_1(0)$	$Y_1(0)$	$X_2(0)$	$Y_2(0)$	$X_3(0)$	$Y_3(0)$
-20	15	-12	8	5	-9

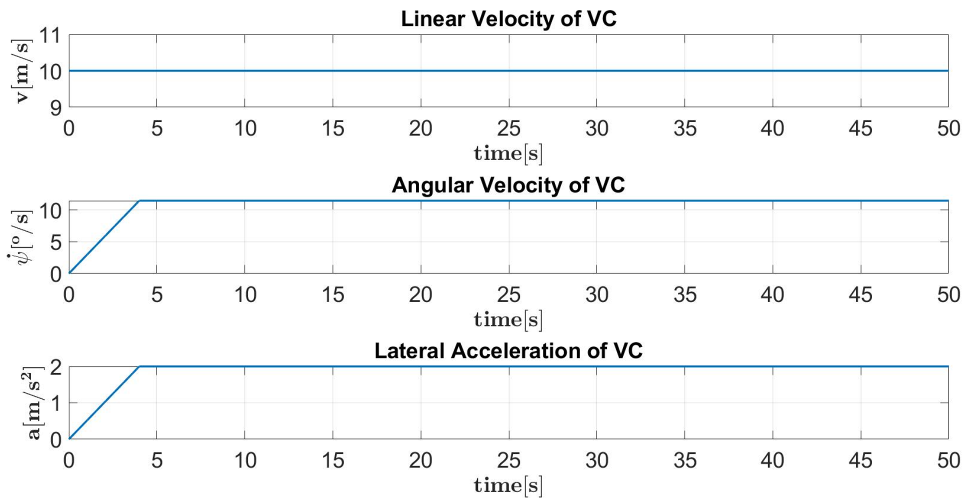

Figure 2.10: Case 2: Linear Velocity, Angular Velocity and Lateral Acceleration of Virtual Car

Again, Figure 2.11 and 2.12 show that the vehicles successfully approach the desired formation. In addition, it has to be pointed out that the the vehicles travel with a non-zero angular velocity on the desired circular path.

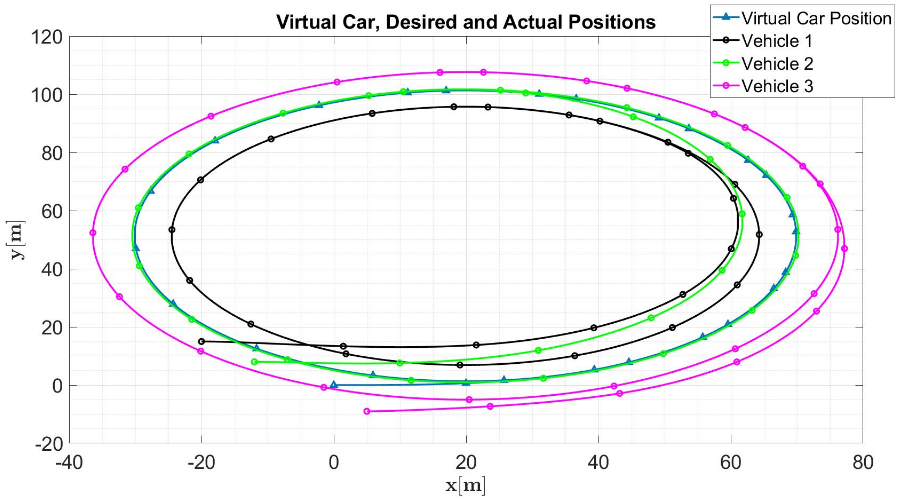

Figure 2.11: Case 2: Position of Vehicles and Virtual Car

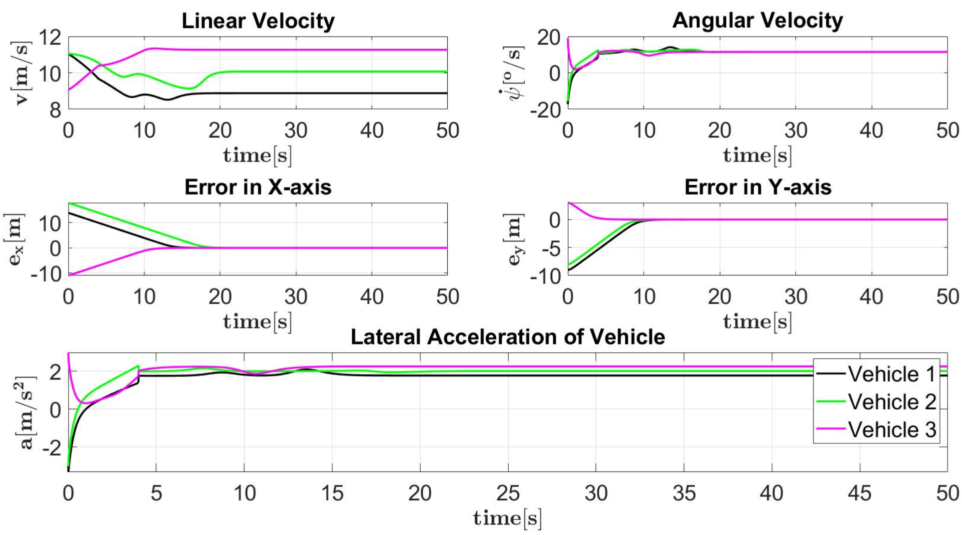

Figure 2.12: Case 2: Linear and Angular Velocity, Error in X and Y Direction and Lateral Acceleration of Vehicles

2.3.3 Case 3

In the third test case, we consider that the virtual vehicle both changes its longitudinal velocity and performs turns in different directions.

Table 2.4: Case 3: Desired and Initial Positions

x_1^{des}	y_1^{des}	x_2^{des}	y_2^{des}	x_3^{des}	y_3^{des}
-8	8	5	0	-8	-8
$X_1(0)$	$Y_1(0)$	$X_2(0)$	$Y_2(0)$	$X_3(0)$	$Y_3(0)$
-30	30	-20	15	15	30

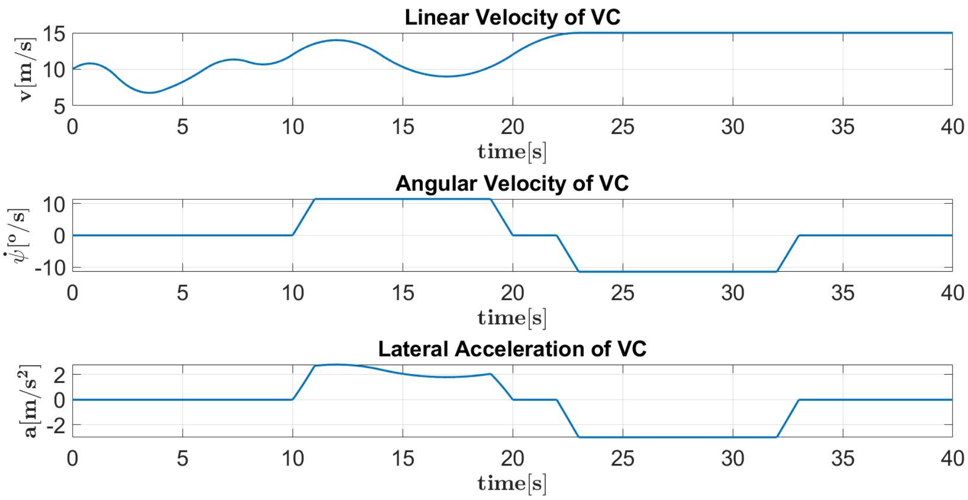

Figure 2.13: Case 3: Linear Velocity, Angular Velocity and Lateral Acceleration of Virtual Car

Similarly to the previous cases, all vehicles follow the desired formation after a short transition from the initial state. Hereby, it has to be noted that, despite the variations in the longitudinal and angular velocity of the virtual vehicle, only minor deviations from the desired trajectory are observed after the transient phase.

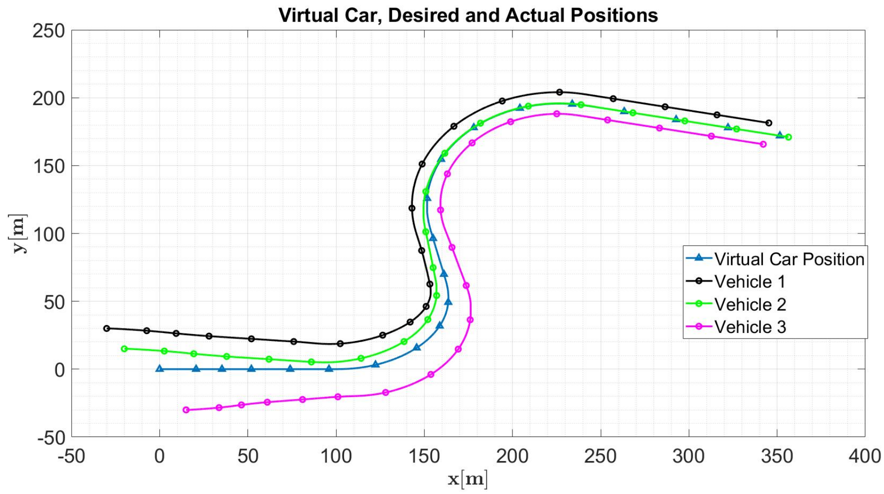

Figure 2.14: Case 2: Position of Vehicles and Virtual Car

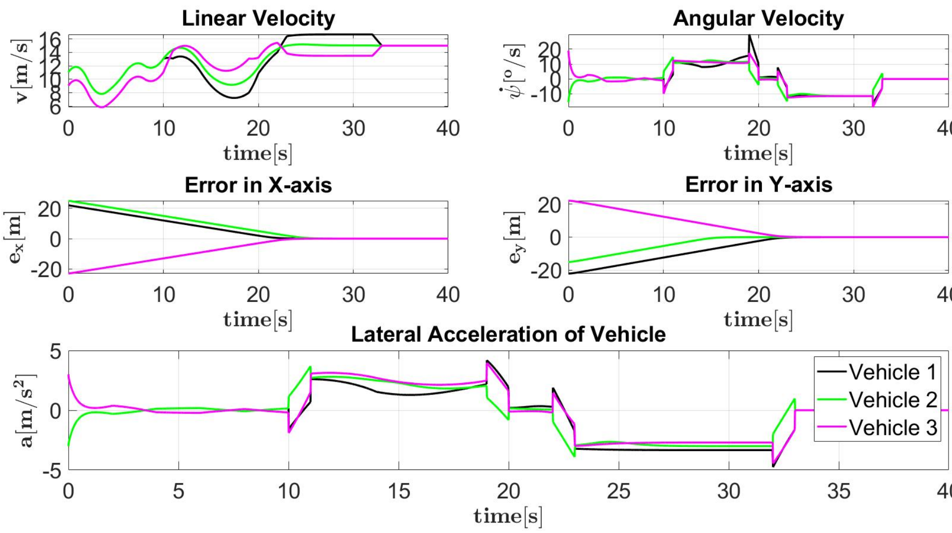

Figure 2.15: Case 3: Linear and Angular Velocity, Error in X and Y Direction and Lateral Acceleration of Vehicles

2.3.4 Discussion

It has to be noted that the described method relies on the usage of a simple kinematic vehicle model that allows direct adjustments of the vehicle's longitudinal and angular velocity as control inputs. The main aim of this thesis is the extension of the described method to a dynamic and hence more realistic vehicle model.

CHAPTER 3

FORMATION CONTROLLER DESIGN FOR A REALISTIC VEHICLE MODEL

In this chapter, the dynamic bicycle vehicle model is derived to be able to test the formation controller described in Section 2.3 with a realistic vehicle model instead of a kinematic model. Furthermore, a tire model which is used frequently in the literature is introduced to model the cornering force. Basic controllers for linear and angular velocity are designed for the dynamic vehicle model to follow the path found by the formation controller. Finally, the formation control performance with the dynamic model is compared with the kinematic model via simulations.

3.1 Dynamic Car Model

In this section, the dynamic model of a nonholonomic 4-wheeled vehicle is introduced due to the need for a more realistic vehicle model than the kinematic model which is used in Section 2.3. The dynamic vehicle model is based on the Dynamic Bicycle Model.

3.1.1 Dynamic Bicycle Model

The Dynamic bicycle Model is the most simple dynamic vehicle model in the literature [36]. The dynamic vehicle model in this study is based on a bicycle car model which is studied by Ardm in [1]. Ardm used the dynamic bicycle model which is represented in Figure 3.1. There are two different coordinate frames which are global coordinates (X, Y and Ψ) and body coordinates (x, y and ψ), which are originated in

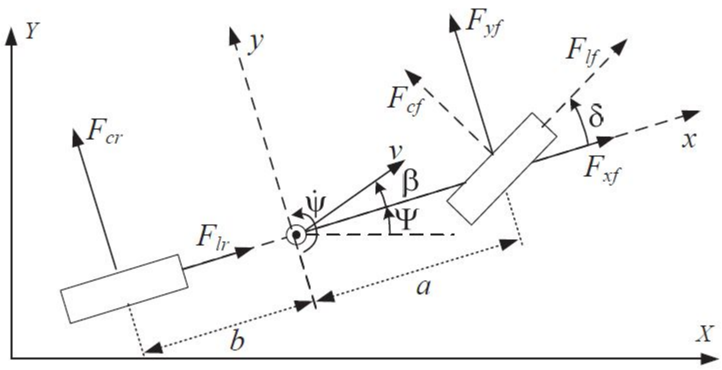

Figure 3.1: Dynamic Bicycle Model

the center of gravity of the car.

In order to control the vehicle model shown in Figure 3.1 in the global coordinate frame, linear and angular speed of the car must be manipulated by changing the motor traction force (F_{lf}) and the steering angle of the front wheels (δ). State equations for the linear speed and the slip angle β of the vehicle are given in (3.1) and (3.2) [1].

$$\dot{v} = \cos(\beta)\frac{F_{lf}\cos(\delta) - F_{cf}\sin(\delta)}{m} + \sin(\beta)\frac{F_{lf}\sin(\delta) + F_{cf}\cos(\delta) + F_{cr}}{m} \tag{3.1}$$

$$\dot{\beta} = \frac{(F_{lf}\sin(\delta) + F_{cf}\cos(\delta) + F_{cr})\cos(\beta)}{mv} - \dot{\psi}\cos^2(\beta) \tag{3.2}$$

In addition, the angular speed of the vehicle ($\dot{\psi}$) is the remaining state in the model which is equated in (3.3):

$$\ddot{\psi} = \frac{(F_{lf}\sin(\delta) + F_{cf}\cos(\delta))a - F_{cr}b}{I_{zz}} \tag{3.3}$$

The forces in these equations are listed below:

- F_{lf}: Traction force provided by the engine,
- F_{cf}: Cornering force on front tire,
- F_{lr}: Longitudinal force on rear tire,
- F_{cr}: Cornering force on rear tire.

It should be noted that the vehicle model used in this study is actuated at the front tire. Therefore, there is no longitudinal force on the rear tire such that $F_{lr} = 0$.

Parameters for a passenger vehicle which can be seen in Table 3.1 are also used by Rucco in 2014 [2]. The dynamic vehicle in the simulations is modeled with the constants below:

Table 3.1: Model Parameters for a Passenger Vehicle

$m[kg]$	$I_{zz}[kgm^2]$	$a[m]$	$b[m]$
1480	1950	1.421	1.029

3.1.2 Lateral Acceleration

The lateral acceleration (a_y) is an essential indicator of a comfortable ride [37]. The lateral acceleration of the car is proportional to the square of the vehicle's linear speed and inversely proportional to the radius of the curve where the vehicle is traveling as can be seen in (3.4)

$$a_y = \frac{v^2}{r}. \tag{3.4}$$

the curve radius (r) can be calculated as below, where v stands for the linear velocity and w stands for the angular velocity of the vehicle:

$$r = \frac{v}{w}. \tag{3.5}$$

By substituting (3.5) into (3.4), the lateral acceleration can be calculated as

$$a_y = v \cdot w. \tag{3.6}$$

In [37], the levels of ride comfort are introduced, which are comfortable, medium comfortable and uncomfortable. Limit values of the lateral acceleration of these levels are $1.8\,\text{m/s}^2$, $3.6\,\text{m/s}^2$ and $5\,\text{m/s}^2$. In this study, a passenger type vehicle's parameters are used. In [38], tests are run for a passenger car and characteristics of ride are evaluated for several road types like highways with different lane amounts and mountain roads. In highways where formation control is more likely to be used, lateral acceleration did not exceed the medium comfort limit of $3.6\,\mathrm{m/s^2}$. Therefore, the lateral acceleration of vehicles is kept within the comfort and medium comfort zones.

3.1.3 Tire Model

The cornering force in the model mentioned in section 3.1.1 is created due to the dynamic nature of tires. Therefore, a tire model is needed to model a realistic vehicle as a dynamic system. Pacejka [39, 40] suggested a semi-empirical and nonlinear model for tire modeling. In this model, the tire's cornering force depends on the slip angle.

The slip angle is described as the angle between the wheel's pointing vector and the wheel's actual movement vector [39]. In Figure 3.2, it can be seen how the slip angle occurs due to the deflection of the structure of the tire while steering the wheel. That is, indeed, the cornering force on tires results from the slip angle.

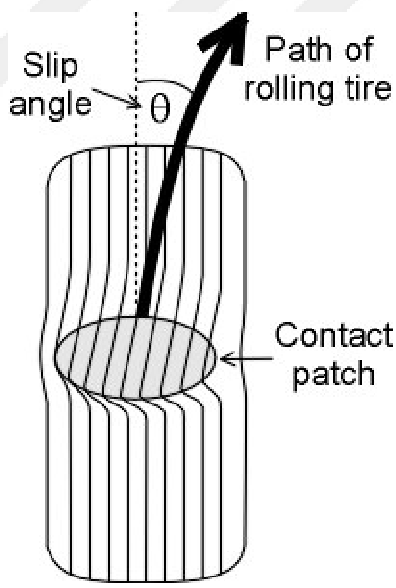

Figure 3.2: Slip Angle due to Distortion of Tire

The slip angle is calculated as the angle between the forward velocity vector and lateral velocity vector. The resulting equation for slip angles of forward and rear tires using local coordinates of the dynamic bicycle model are given in (3.7) and (3.8) respectively [1].

$$\alpha_f = \tan^{-1}(\frac{\dot{y} + a\dot{\psi}}{\dot{x}}) - \delta \tag{3.7}$$

$$\alpha_r = \tan^{-1}(\frac{\dot{y} - b\dot{\psi}}{\dot{x}}) \tag{3.8}$$

For the cornering force calculation, Pacejka [39,40] came up with the Magic Formula for front and rear tires which can be seen in (3.9) and (3.10). The magic formula is frequently used in the literature [2,41,42].

$$F_{cf} = D\sin(C\tan^{-1}(B\alpha_f - E(B\alpha_f - \tan^{-1}(B\alpha_f)))) \tag{3.9}$$

$$F_{cr} = D\sin(C\tan^{-1}(B\alpha_r - E(B\alpha_r - \tan^{-1}(B\alpha_r)))) \tag{3.10}$$

In these equations, α_f and α_r are the slip angles of front and rear tires, respectively. Also, B, C, D and E are constants, which depend on each tire's nature. Here, the constant D is related to the road friction coefficient (μ) and the total weight on a tire calculated in (3.11).

$$D = \mu m g. \tag{3.11}$$

The cornering force is illustrated with varying parameters in the Magic Formula. Each coefficient in the Magic Formula changes a different characteristic of the cornering force. In Figure 3.3, it can be seen that by changing parameter B, the angle in which the maximum/minimum force location appears can be changed. For large slip angle values, the saturation value level of the cornering force can be manipulated by varying C as can be seen in Figure 3.4. The maximum force can be adjusted by the parameter D as can be seen in Figure 3.5. Finally, the curve sharpness changes with the parameter E which can be seen in Figure 3.6.

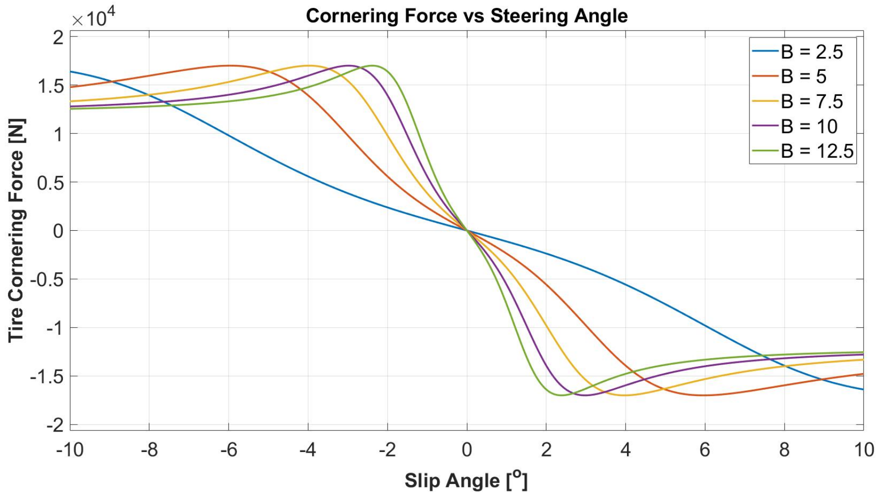

Figure 3.3: Cornering Force vs Steering Angle for Varying B Coefficient

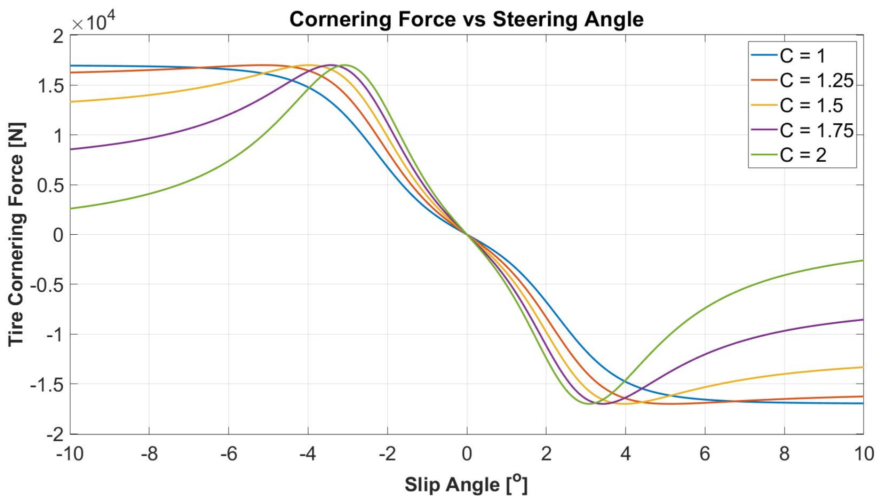

Figure 3.4: Cornering Force vs Steering Angle for Varying C Coefficient

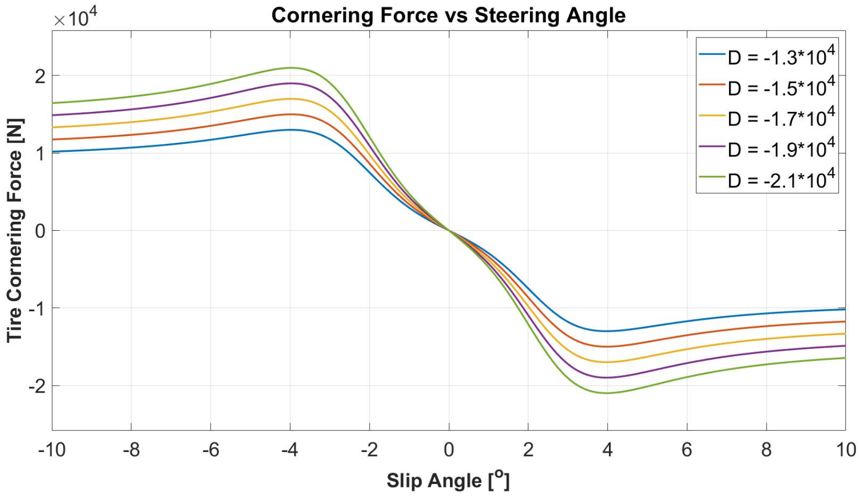

Figure 3.5: Cornering Force vs Steering Angle for Varying D Coefficient

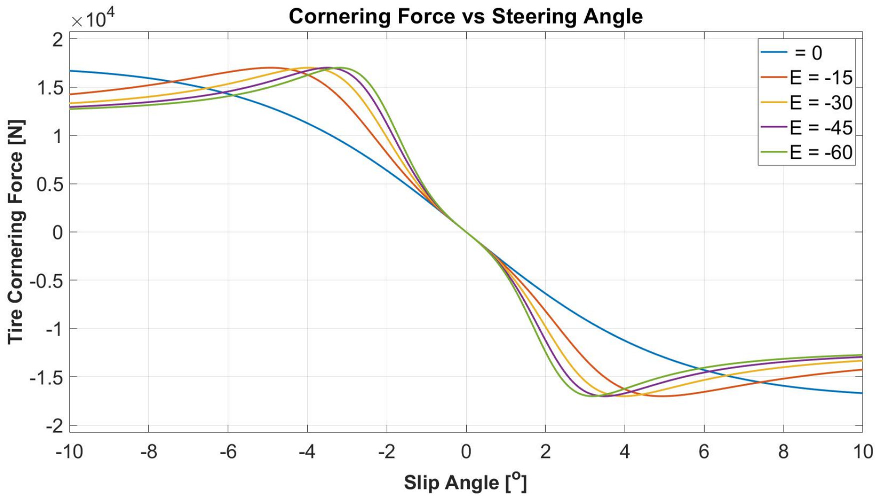

Figure 3.6: Cornering Force vs Steering Angle for Varying E Coefficient

From now on, parameters from [1, 2] in Table3.2 are used for Magic Formula to calculate cornering force on tires. Also, it is assumed that front and rear tires are exactly same. The resultant cornering force with respect to slip angle is illustrated in Figure 3.7.

Table 3.2: Magic Formula Parameters [1,2]

B	C	D	E
8.22	1.65	$-1.7 \cdot 10^4$	-10

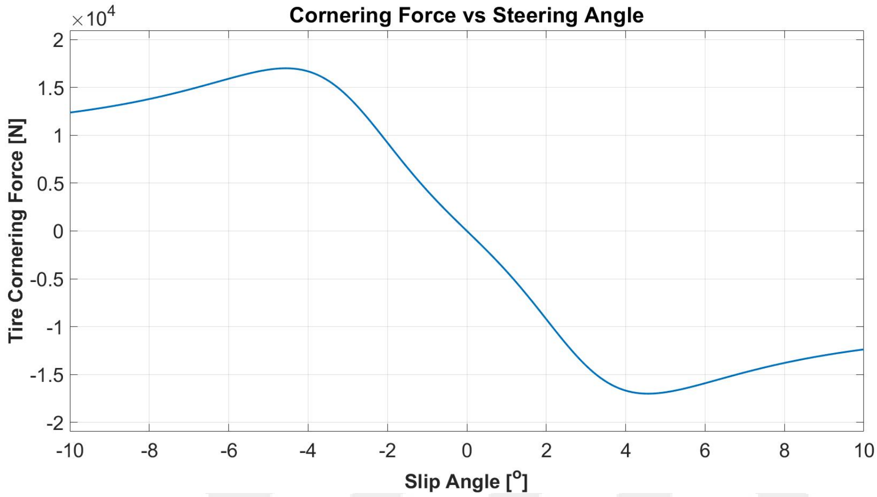

Figure 3.7: Cornering Force vs Steering Angle

The nonlinear characteristics of the tire cornering force have already been examined previously. In Figure 3.7, it can be seen that tires start to slip when the slip angle exceeds $4°$. However, the cornering force behaves as it is linear for slip angles below $4°$. Therefore, if it is assumed that the slip angle will never exceed the critical angle of $4°$, a linear formula for the cornering force can be used.

In order to linearize Magic Formula described in (3.9), The Taylor Series is used for the slip angle around the origin ($\alpha = 0$) and the linearized equation can be seen below.

$$F_c = B \cdot C \cdot D \cdot \alpha. \tag{3.12}$$

Results for the linearized Magic Formula are illustrated in Figure 3.8. It can be clearly seen that for slip angles below $4°$, (3.12) can be used instead of the Magic Formula for modeling the cornering force.

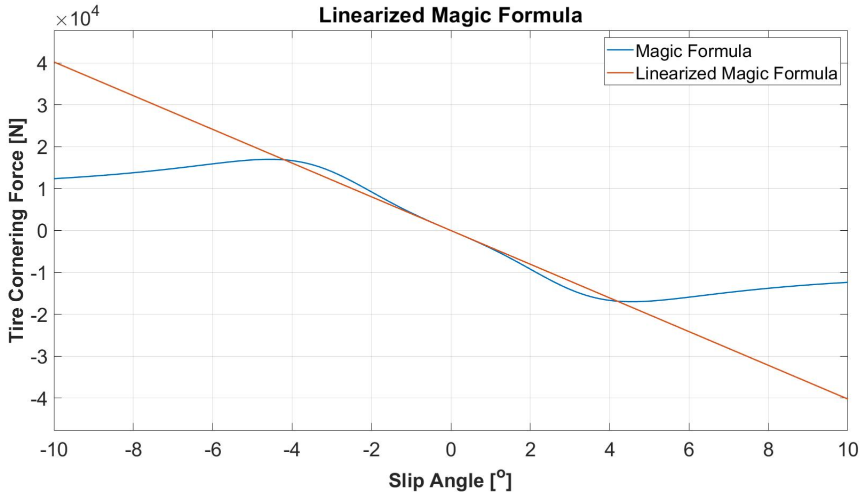

Figure 3.8: Magic Formula vs Linearized Magic Formula

3.1.4 Motor Traction Force

As mentioned in Section 3.1.1, the motor traction force F_{lf} is one of the inputs of the dynamic bicycle model. In Ardm's study [1], F_{lf} is calculated as in (3.13).

$$F_{lf} = \frac{ma_r - F_{cf}(\cos(\delta)\sin(\beta) - \sin(\delta)\cos(\beta)) - F_{cr}\sin(\beta)}{\cos(\delta)\cos(\beta) + \sin(\delta)\sin(\beta)} \tag{3.13}$$

For the calculation of the motor traction force, F_{cf} and F_{cr} are explained in Section 3.1.1. a_r is the desired acceleration of the vehicle. Therefore, the required motor traction force (F_{lf}) can be directly calculated from the desired acceleration, which can then be considered as the input of the system instead of the motor traction force even during maneuvers ($\delta \neq 0$).

In this study, it is assumed such that the motor of the car can give any amount of traction force. However, although the motor of the vehicle can generate sufficient force for the required control effort, there is a limit, where too much force can make the tires spinning so that the car can not accelerate as expected. The aximum traction effort that avoids tires from spinning depends on the road surface's adhesion, rolling resistance, vehicle's characteristics and linear speed of the vehicle. For front-wheeldrive vehicles, the maximum traction force can be seen in (3.14) [43].

$$F_{lf}{}^{max} = \frac{\mu W(a + f_{rl}h)/(a+b)}{1 + \mu h/(a+b)}. \tag{3.14}$$

Here,

μ = coefficient of road adhesion,

W = weight of car,

f_{rl} = coefficient of rolling resistance,

h = height of center of gravity.

The coefficient of road resistance for a road vehicle driven on paved surface can be calculated with respect to the vehicle speed as

$$f_{rl} = (0.01)(1 + \frac{V}{40.8}). \tag{3.15}$$

In Table 3.3, the maximum coefficient of road adhesion values according to the road condition are given. In Figure 3.9, the maximum traction force with respect to the vehicle speed for varying road adhesion coefficients is illustrated.

Table 3.3: Typical Road Adhesion Coefficients

Pavement	Maximum Coefficient of Road Adhesion
Good, dry	1.00
Good, wet	0.90
Poor, dry	0.80
Poor, wet	0.60
Ice	0.25

In this study, pavement's condition is assumed as good and dry in Table 3.3 ($\mu = 1$). Also, the vehicle's height of center of gravity is chosen as 0.55 meters from the road level [43].

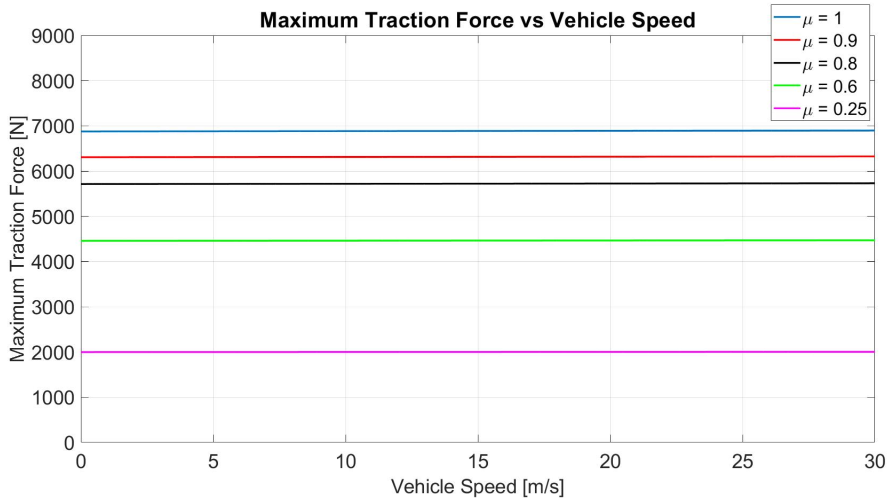

Figure 3.9: Maximum Track Force vs Vehicle Speed for Different Road Adhesion Coefficients

3.1.5 Friction Circle

The friction circle describes the fact that the longitudinal and lateral forces on the tire are limited by each other [39]. For a real-world tire, lateral and longitudinal force does not limit each other equally so it is more suitable to use the term "friction ellipse". However, for this work it is assumed for simplicity that they are limited equally. The resulting limitation is equated in (3.16). In this inequality, a_{long} and a_{lat} refers to the longitudinal and lateral acceleration, while μ stands for the friction coefficient of the road and g stands for gravitational constant.

$$a_{long}^2 + a_{lat}^2 < \mu^2 g^2 \tag{3.16}$$

The friction coefficient is taken as 1, which represents dry-asphalt. As mentioned Section 3.1.2, the lateral acceleration is limited as $3.6\,\mathrm{m/s^2}$ in this work. For a comfortable ride, the longitudinal acceleration should be less than $2\,\mathrm{m/s^2}$ [44–46]. However, for some cases in this work, the longitudinal acceleration can reach up to $5\,\mathrm{m/s^2}$ due to the linear velocity controller's performance which is mentioned in Section 3.2.1. As a result, it must be noted that the friction circle is not violated in any case throughout the thesis work.

3.1.6 Simulation Results for Nonlinear Bicycle Model

The nonlinear model has three states and two inputs which are already explained in Section 3.1.1. In (3.17), x defines these states and u defines the inputs. Furthermore, as the motor traction force F_{lf}, (3.13) is being used.

$$x = \begin{bmatrix} v \\ \beta \\ \dot{\psi} \end{bmatrix} \quad \text{and} \quad u = \begin{bmatrix} F_{lf} \\ \delta \end{bmatrix} \tag{3.17}$$

In (3.18), the functions f_1, f_2 and f_3 are already given in (3.1), (3.2) and (3.3), respectively.

$$\dot{x} = \begin{bmatrix} \dot{v} \\ \dot{\beta} \\ \ddot{\psi} \end{bmatrix} = \begin{bmatrix} f_1 \\ f_2 \\ f_3 \end{bmatrix} \tag{3.18}$$

Therefore, the overall model is as stated below:

$$x = \begin{bmatrix} \int \dot{v} \\ \int \dot{\beta} \\ \int \ddot{\psi} \end{bmatrix} \tag{3.19}$$

Since the Cartesian coordinate system is used as global coordinate frame for the nonlinear formation controller, the vehicle's movement should be converted to the Cartesian coordinates as below:

$$\dot{x} = v \cos(\beta) \tag{3.20}$$

$$\dot{y} = v \sin(\beta) \tag{3.21}$$

(3.20) and (3.21) are defining the speed in x and y directions in the body coordinate frame. In order to find the vehicle's speed in X and Y directions in the global coordinate frame, the equations below are used:

$$\dot{X} = \dot{x} \cos(\psi) - \dot{y} \sin(\psi) \tag{3.22}$$

$$\dot{Y} = \dot{x} \sin(\psi) + \dot{y} \cos(\psi) \tag{3.23}$$

Finally, the positions can be calculated by integrating (3.22) and (3.23) as below:

$$X = X_0 + \int_t \dot{x}\, dt \tag{3.24}$$

$$Y = Y_0 + \int_t \dot{y}\, dt \tag{3.25}$$

In the subsequent figures, simulations of the nonlinear bicycle model can be seen for different inputs. Figure 3.10 displays the case of a non-zero steering input and zero acceleration. The corresponding vehicle position is shown in Figure 3.11 and the related speeds and lateral accelerations can be seen in Figure 3.12. Furthermore, Figure 3.13 shows that the slip angle remains limited.

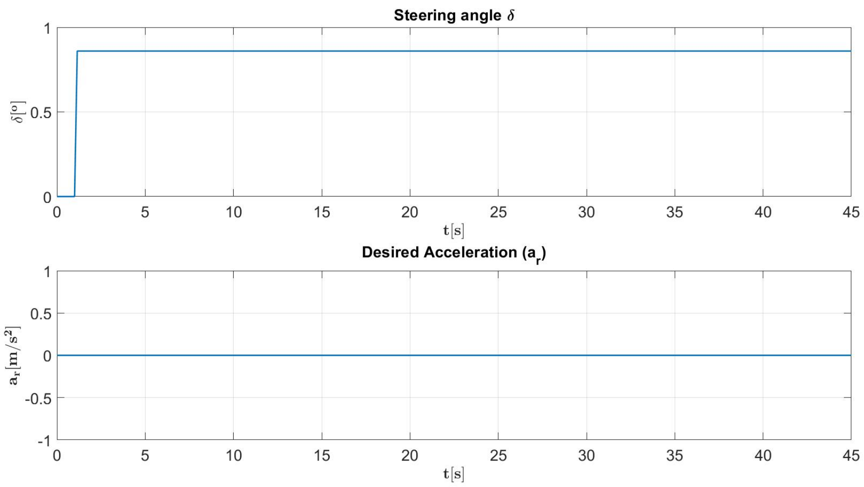

Figure 3.10: Case 1: Steering Angle and Desired Acceleration as Inputs

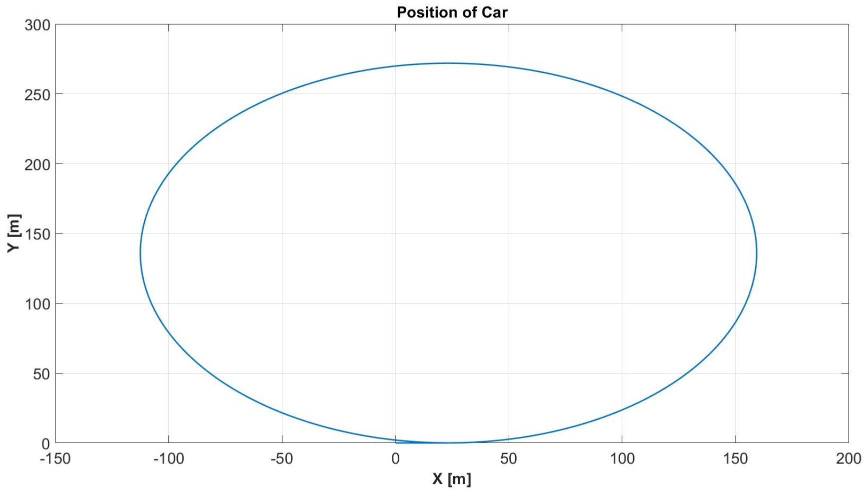

Figure 3.11: Case 1: Position of Car

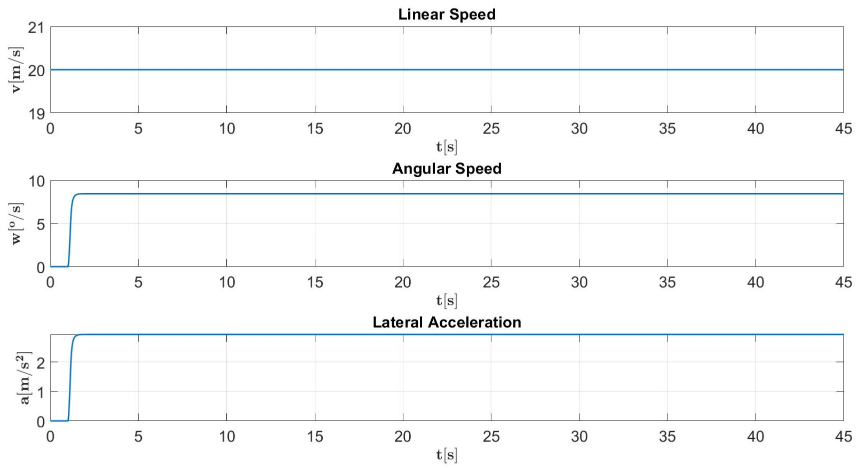

Figure 3.12: Case 1: Linear Velocity, Angular Velocity and Lateral Acceleration of Car

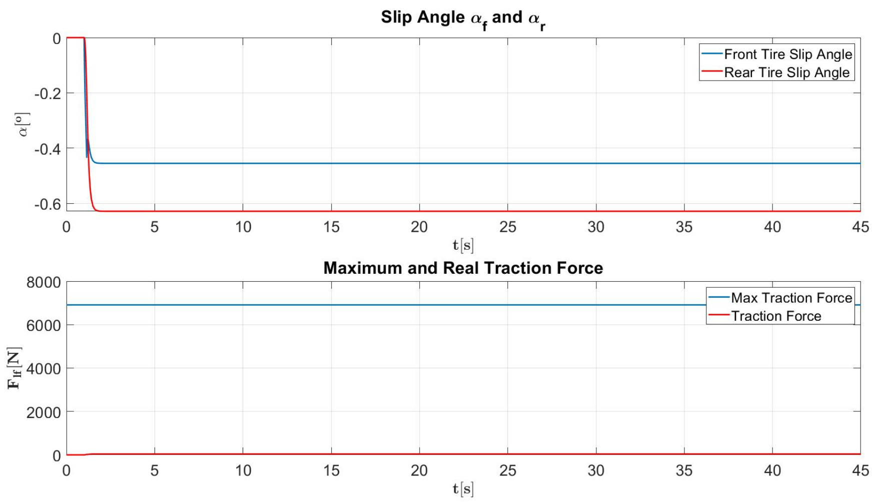

Figure 3.13: Case 1: Slip Angles of Front/Rear Tires and Motor Traction Force

Figure 3.14 considers the case of fluctuations in the steering angle and the desired acceleration. The simulation results in Figure 3.15 to 3.17 show the related vehicle signals.

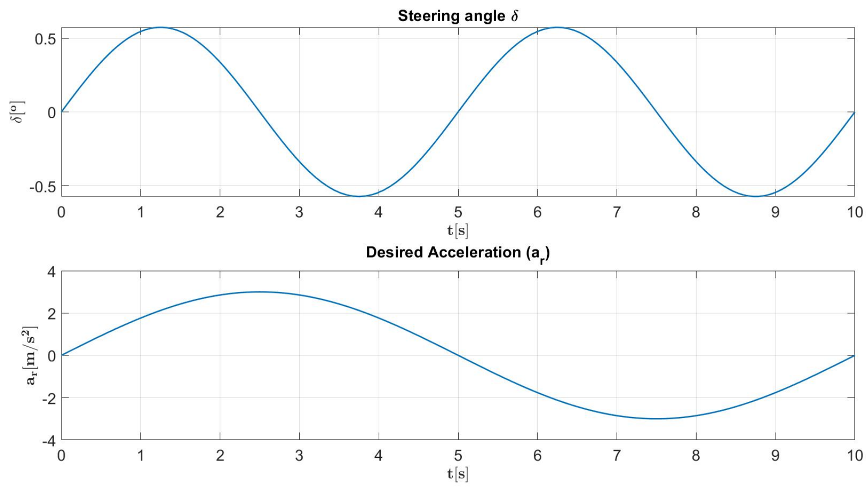

Figure 3.14: Case 2: Steering Angle and Desired Acceleration as Inputs

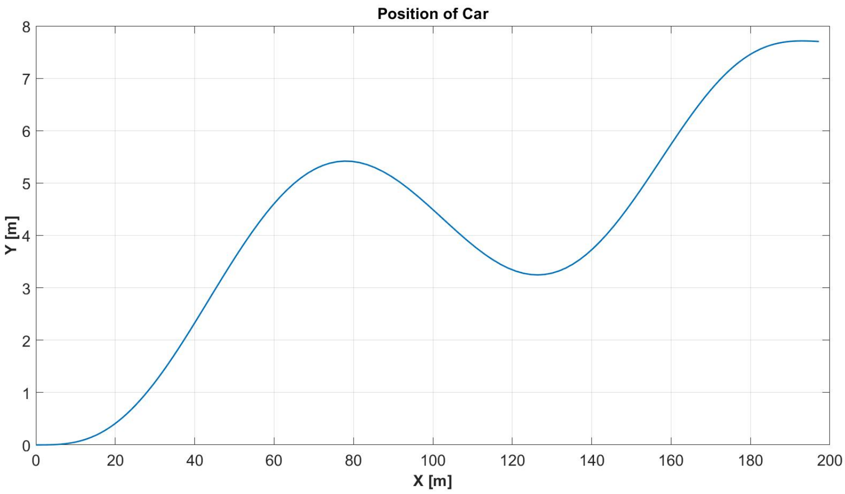

Figure 3.15: Case 2: Position of Car

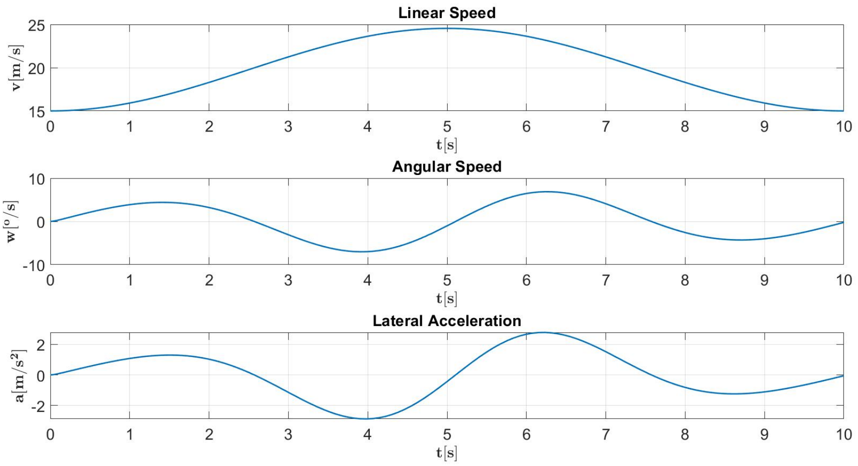

Figure 3.16: Case 2: Linear Velocity, Angular Velocity and Lateral Acceleration of Car

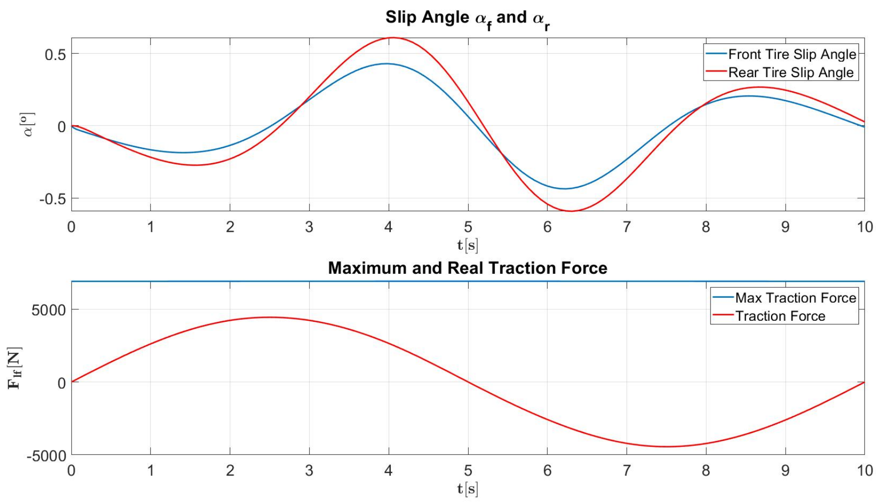

Figure 3.17: Case 2: Slip Angles of Front/Rear Tires and Motor Traction Force

Finally, we apply the inputs in Figure 3.18 with abrupt changes in the steering angle and desired acceleration. Figure 3.19 to 3.21 again confirm the intuitively expected reaction of the vehicle to the applied inputs.

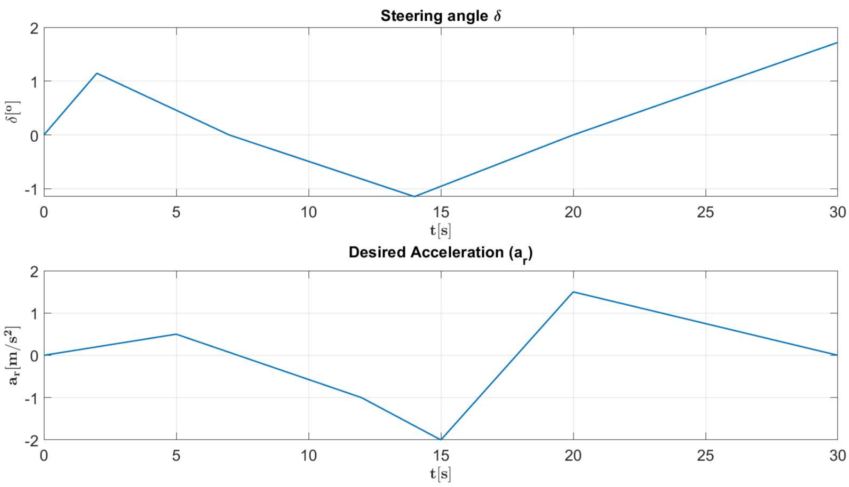

Figure 3.18: Case 3: Steering Angle and Desired Acceleration as Inputs

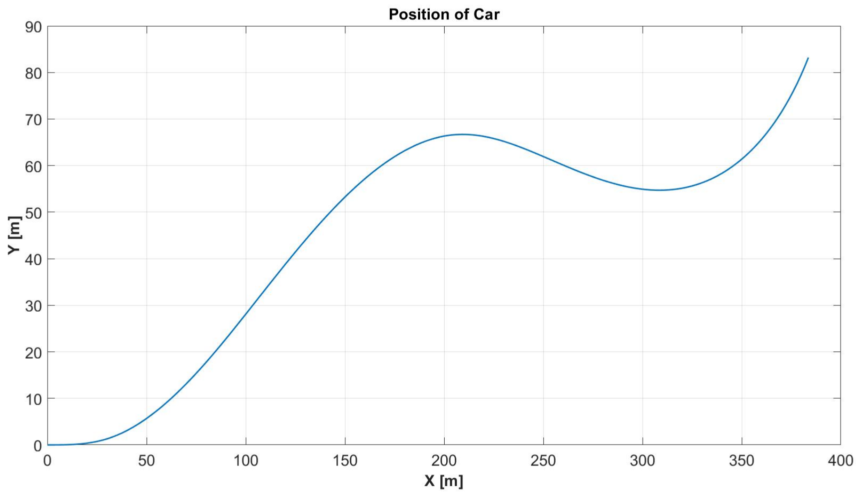

Figure 3.19: Case 3: Position of Car

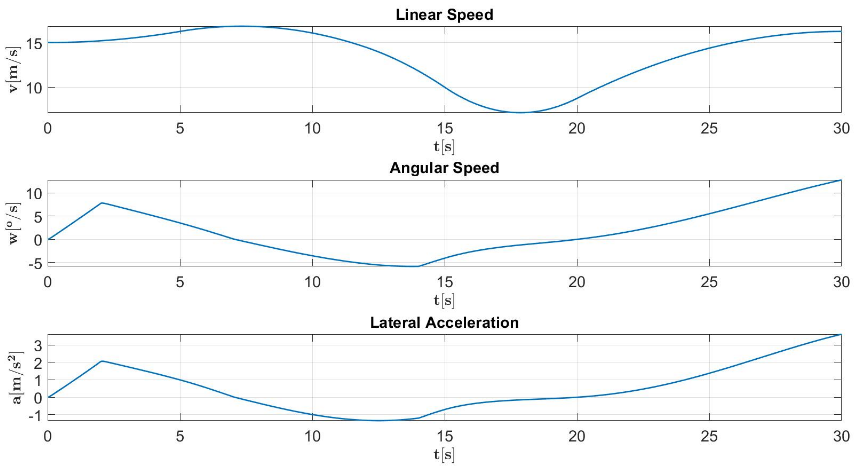

Figure 3.20: Case 3: Linear Velocity, Angular Velocity and Lateral Acceleration of Car

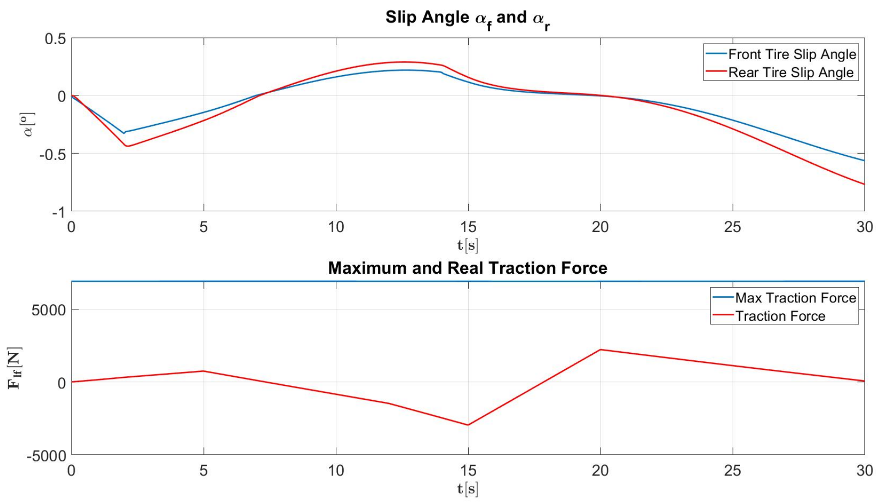

Figure 3.21: Case 3: Slip Angles of Front/Rear Tires and Motor Traction Force

3.1.7 Linear Dynamic Bicycle Model

If a linear model can be obtained from the nonlinear bicycle car model, linear techniques can be used in order to control the vehicle movement with reference signals from the formation controller. To linearize the bicycle model, (3.1), (3.2) and (3.3) are used, where (3.13) and (3.12) are inserted.

The resulting equations are linearized using the Taylor Series around the point with zero steering angle and the car moves at a constant speed. In other words, the chosen equilibrium point is $v = v_{lin}$ (constant speed), $\beta = 0$, $\dot{\psi} = 0$, $\delta = 0$, $a_r = 0$. The equations of the linearized model are given in (3.26), (3.27) and (3.28).

$$\dot{v} = a_r \tag{3.26}$$

$$\dot{\beta} = \beta\frac{2BCD}{mv} + \dot{\psi}(\frac{BCD(a-b)}{mv^2} - 1) - \delta\frac{BCD}{mv} \tag{3.27}$$

$$\ddot{\psi} = \beta\frac{BCD(a-b)}{I_{zz}} + \dot{\psi}\frac{BCD(a^2+b^2)}{I_{zz}} - \delta\frac{BCDa}{I_{zz}} \tag{3.28}$$

For a constant speed such as v, the resulting linear state-space model becomes like in equation (3.29).

$$\begin{bmatrix}\dot{v}\\ \dot{\beta}\\ \ddot{\psi}\end{bmatrix}=\begin{bmatrix}0 & 0 & 0\\ 0 & \frac{2BCD}{mv} & (\frac{BCD(a-b)}{mv^2}-1)\\ 0 & \frac{BCD(a-b)}{I_{zz}} & \frac{BCD(a^2+b^2)}{I_{zz}}\end{bmatrix}\begin{bmatrix}v\\ \beta\\ \dot{\psi}\end{bmatrix}+\begin{bmatrix}0 & 1\\ \frac{BCD}{mv} & 0\\ \frac{BCDa}{I_{zz}} & 0\end{bmatrix}\begin{bmatrix}\delta\\ a_r\end{bmatrix} \tag{3.29}$$

In addition, it can be noted that it is possible to remove v from the linear state space model since it is the integral of a_r. The resulting reduced state space model is shown in (3.30).

$$\begin{bmatrix}\dot{\beta}\\ \ddot{\psi}\end{bmatrix}=\begin{bmatrix}\frac{2BCD}{mv} & (\frac{BCD(a-b)}{mv^2}-1)\\ \frac{BCD(a-b)}{I_{zz}} & \frac{BCD(a^2+b^2)}{I_{zz}}\end{bmatrix}\begin{bmatrix}\beta\\ \dot{\psi}\end{bmatrix}+\begin{bmatrix}\frac{BCD}{mv}\\ \frac{BCDa}{I_{zz}}\end{bmatrix}\begin{bmatrix}\delta\end{bmatrix} \tag{3.30}$$

It is already stated that the nonlinear model is linearized for a constant velocity v. For this model, the linearization speed is taken as $v = 10\,\text{m/s}$ and the parameters in Tables 3.1 and 3.2 are used. The final model with substituted parameter values can be found in equation (3.31).

$$\begin{bmatrix}\dot{\beta}\\ \ddot{\psi}\end{bmatrix}=\begin{bmatrix}-31.16 & -1.61\\ -46.35 & -36.40\end{bmatrix}\begin{bmatrix}\beta\\ \dot{\psi}\end{bmatrix}+\begin{bmatrix}15.58\\ 168.02\end{bmatrix}\begin{bmatrix}\delta\end{bmatrix} \tag{3.31}$$

To validate the state-space model, the same steering angle input in Figure 3.22 is given to both nonlinear model with linear tire model and linear state-space model. In the first experiment, the linear car speed of both models is fixed to the linearization speed ($v = 10\,\text{m/s}$), which can be seen in Figure 3.22. In Figure 3.23 it can be seen that linear model and nonlinear model are moving very close to each other.

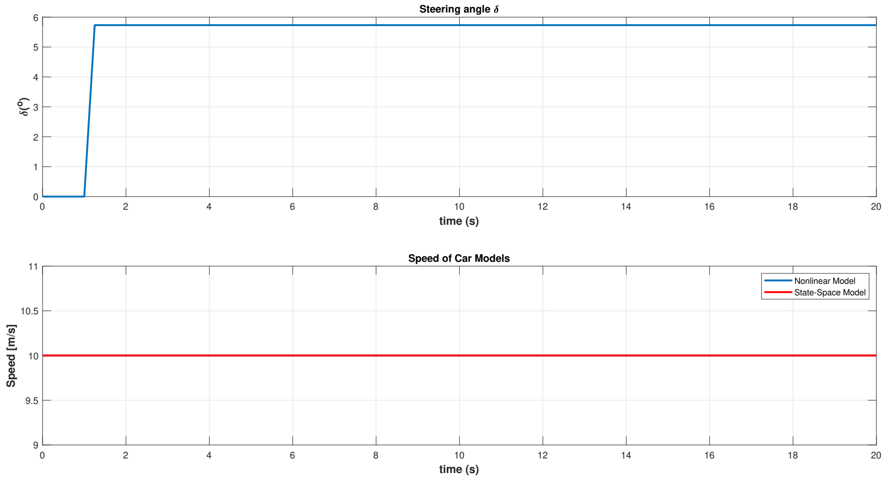

Figure 3.22: Step Steering Input and Car Speed

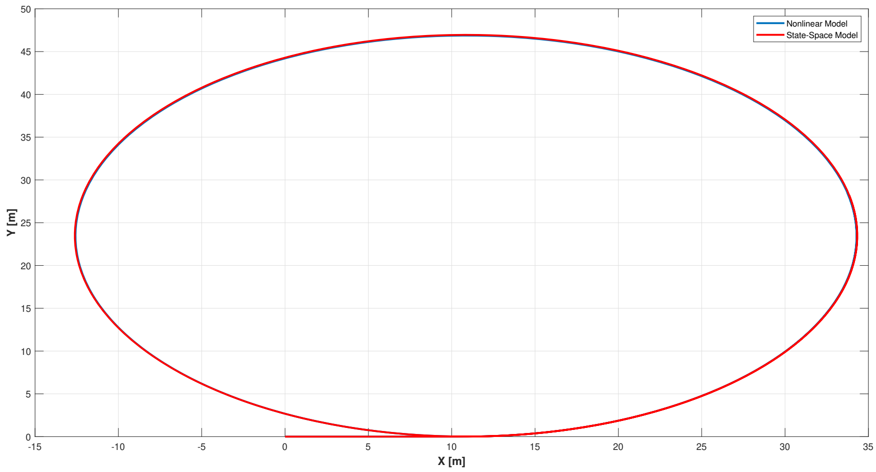

Figure 3.23: Position of Car Models

On the other hand, as the speed of linear car model diverges from the linearization speed, the results from the linear state-space model diverge from the nonlinear model. The same steering angle input as before is given to both models. However, this time desired acceleration is fixed as $a_r = 0.2\,\text{m/s}^2)$ as in Figure 3.24. It can be seen clearly that the resulting positions of the models differ in Figure 3.25. As the speed of the car diverges from the linearization speed, the linear state-space model looses its accuracy.

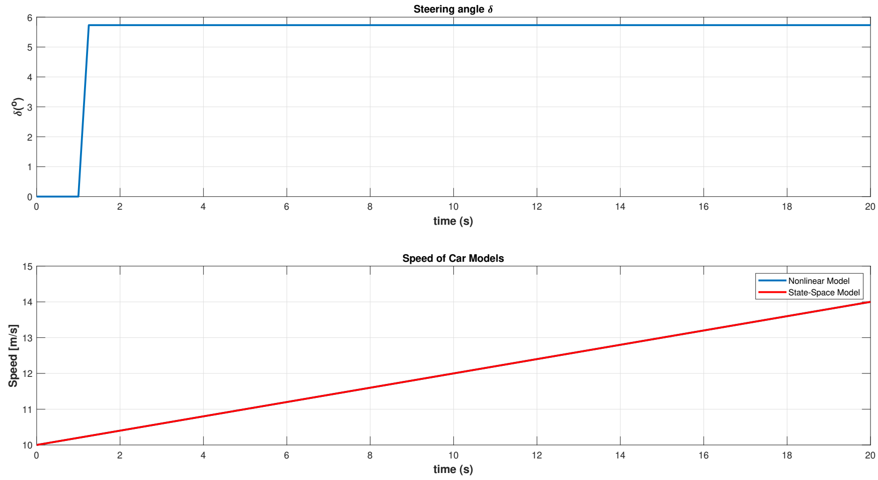

Figure 3.24: Step Steering Input and Car Speed

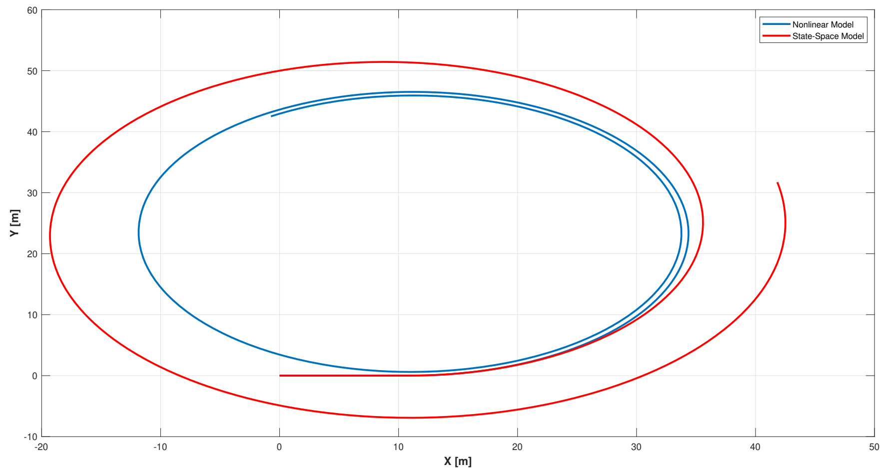

Figure 3.25: Position of Car Models

Since the derived linear model diverges from the nonlinear model after changes in the linear speed of the vehicle, it can not be directly used for vehicle speed controllers. Hence, robust controllers for nonlinear systems will be used for vehicle controllers.

3.2 Vehicle Linear and Angular Speed Controllers

In Section 2.3, the linear and angular speed of AVs are given as output of the nonlinear formation controller and serve as the inputs for the kinematic vehicle model. Nevertheless, linear and angular velocity are states of the dynamic bicycle model and can hence not directly be controlled. In order to apply the reference values for the linear and angular velocity provided by the nonlinear formation controller, we propose the control structure as shown in Figure 3.26. Here, the dynamic bicycle model with the steering angle δ and the desired acceleration a_r as described in Section 3.1.1 is used.

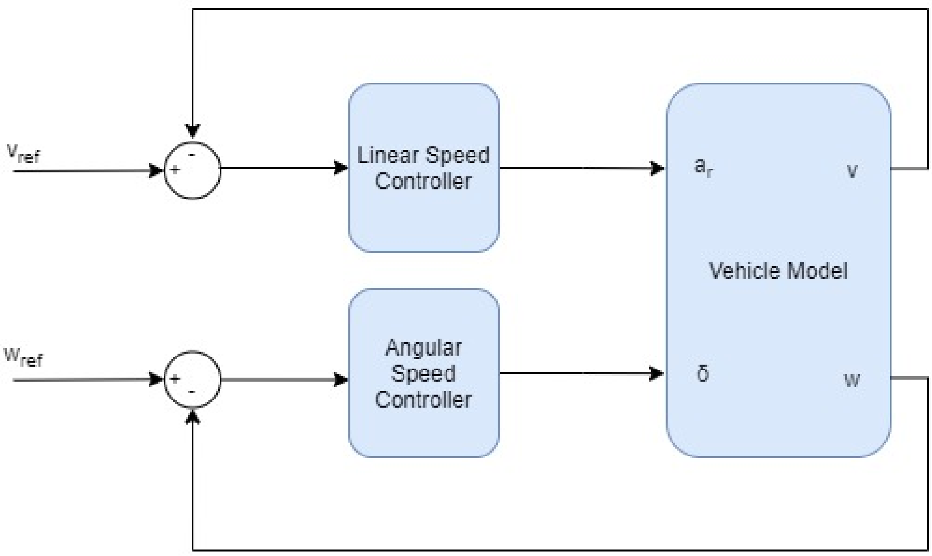

Figure 3.26: Linear and Angular Speed Controllers for Vehicle Model

3.2.1 Linear Velocity Controller

In this section of the study, the development of a linear velocity controller is described. Firstly, the most basic controller which is a P-controller is used as below:

$$a_r = K_p^{lin} e, \tag{3.32}$$

where

$$e = v_{ref} - v \tag{3.33}$$

The P-controller is next evaluated for different coefficient values. As the coefficient of proportional controller gets bigger, the control effort (F_{lf}) gets higher which can be seen in Figures 3.27, 3.28 and 3.29. In Figure 3.29, it can be seen that at the beginning of the simulation where the error is large, the traction force generated by the motor is larger than the threshold which is described in Section 3.1.4.

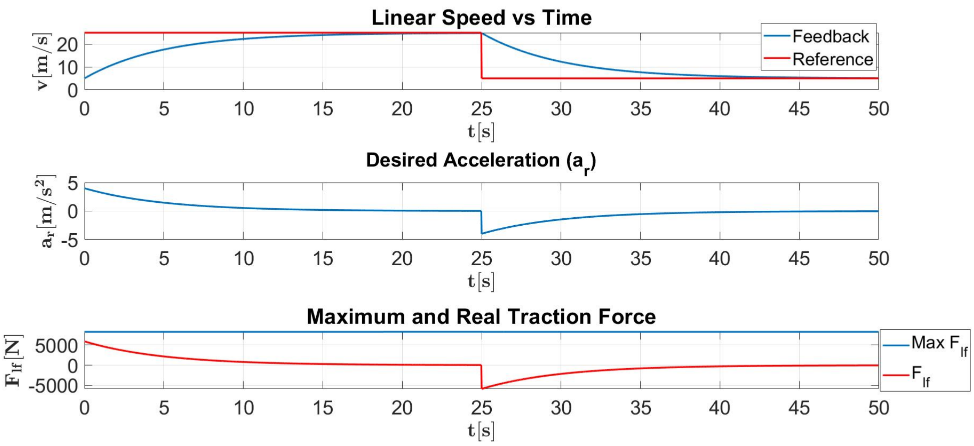

Figure 3.27: Linear Velocity Controller with $K_p^{lin} = 0.2$ for Large Error

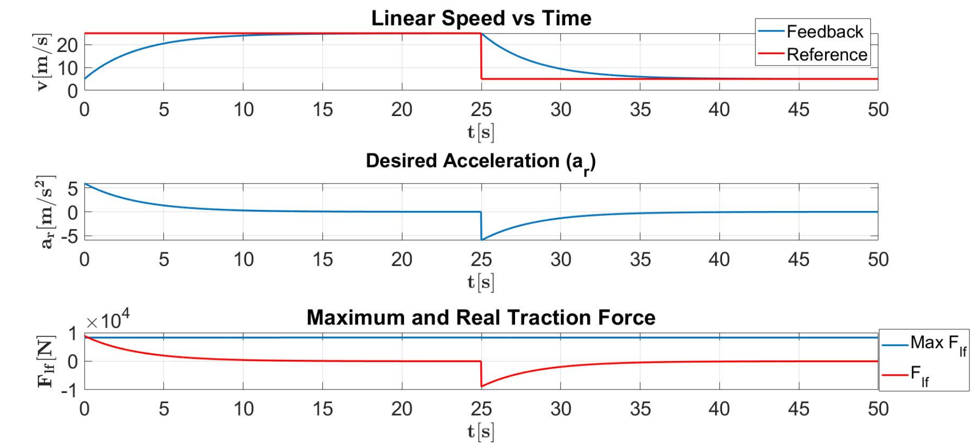

Figure 3.28: Linear Velocity Controller with $K_p^{lin} = 0.3$ for Large Error

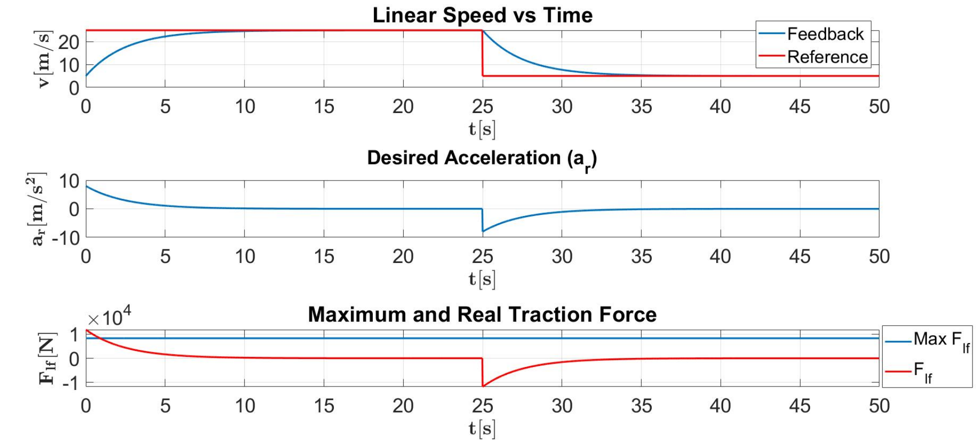

Figure 3.29: Linear Velocity Controller with $K_p^{lin} = 0.4$ for Large Error

However, for smaller errors such as in the cases below (Figures 3.30 and 3.31), the control effort is lower, which results in a slow convergence to the reference signal for the linear velocity of the vehicle.

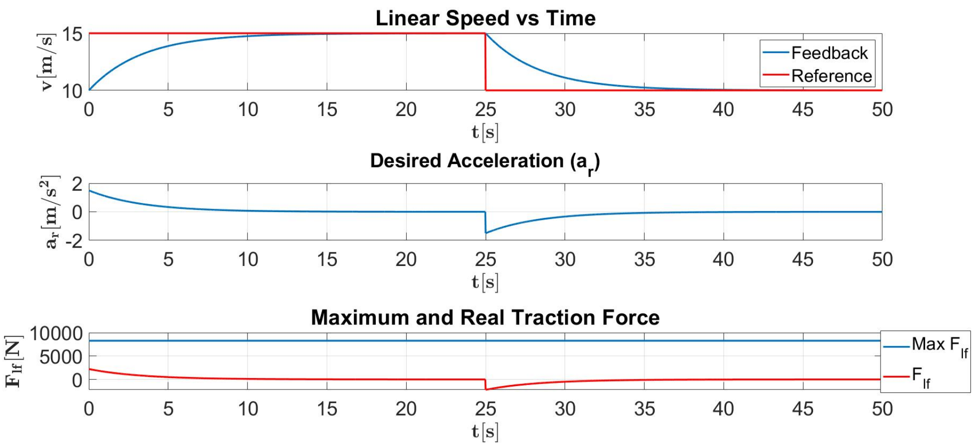

Figure 3.30: Linear Velocity Controller with $K_p^{lin} = 0.3$ for Small Error

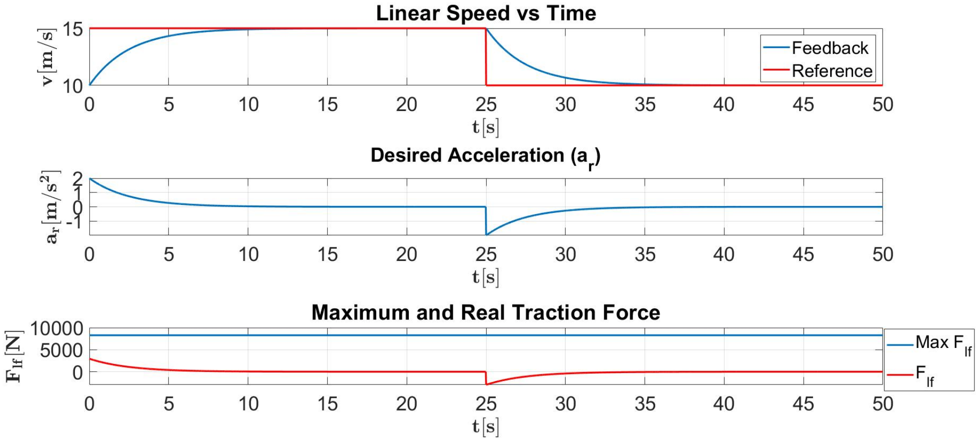

Figure 3.31: Linear Velocity Controller with $K_p^{lin} = 0.4$ for Small Error

Accordingly, a single P-controller for the linear velocity control is not efficient since the controller performance is low for small errors when a small proportional coefficient is chosen such that the control effort, i.e., the motor traction force does not exceed the limit value for large errors. On the other hand, when the coefficient is chosen to be high in order to improve the performance for low errors, the maximum motor traction force is exceeded.

In order to get a satisfactory performance for both low and high errors, a gain scheduler for the P-controller is implemented. The equation for the proportional coefficient with respect to the error can be seen below:

$$K = \frac{G_{max} - G_{min}}{e^{(|error|K_{min})}} + G_{min} \tag{3.34}$$

In Figure 3.32, it can be seen how the proportional constant of P-controller is changed with respect to the error for the gain schedule's parameters in Table 3.4.

Table 3.4: Gain Scheduling Parameters

G_{min}^{lin}	G_{max}^{lin}	K_{min}^{lin}
0.27	8	1

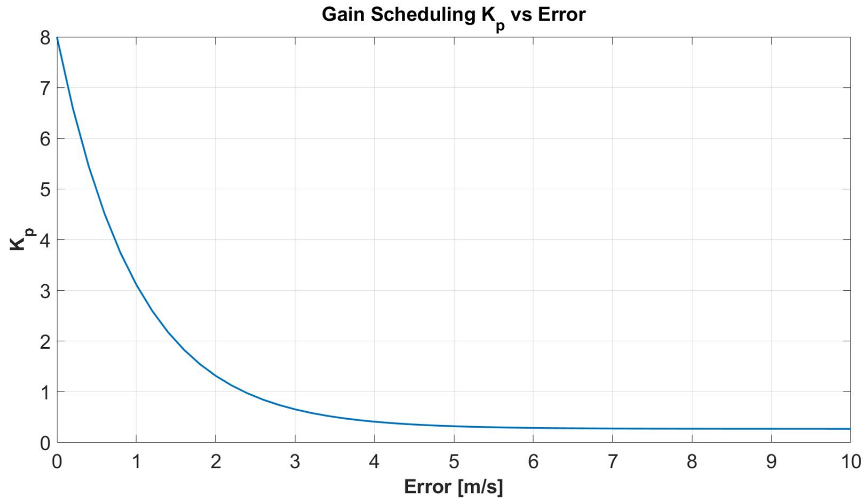

Figure 3.32: Gain Scheduling K_p^{lin} with respect to error of linear velocity

The results of the linear speed controller which is implemented with gain scheduling K_p can be seen in Figure 3.33 and 3.34. For large errors, the motor traction force does not exceed its limit. Furthermore, it can be seen clearly in Figure 3.34 that the controller performance is significantly improved compared to the simple proportional controller for low errors, which is confirmed in Figure 3.30.

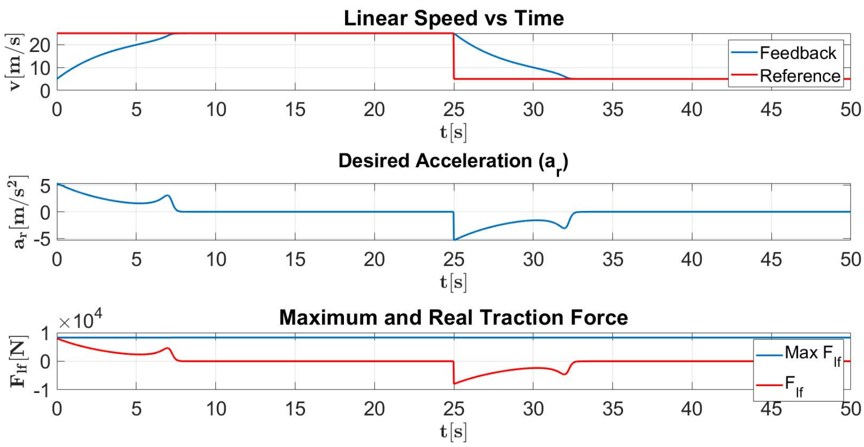

Figure 3.33: Linear Velocity Controller with Gain Schedule for Large Error

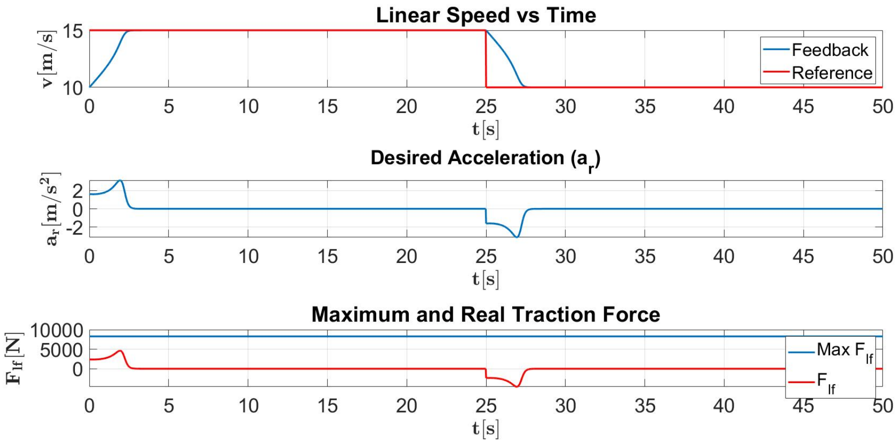

Figure 3.34: Linear Velocity Controller with Gain Schedule for Small Error

The previous experiments were carried out for the parameters of a passenger vehicle. We next look at the parameters of a small truck, whose weight and size are bigger than a passenger vehicle as shown in Table 3.5 [47].

Table 3.5: Model Parameters for a Small Truck

$m[kg]$	$I_{zz}[kgm^2]$	$a[m]$	$b[m]$
7490	4700	1.7	2.55

Since this vehicle is heavier, the traction force supplied by the motor is higher to obtain the same desired acceleration for the passenger type vehicle. Although the motor capacities of these vehicles are bigger, it is natural not to obtain as high acceleration as for small vehicles. Therefore, the linear velocity controller should be tuned for different types of vehicles. The tuned gain scheduled controller parameters for the small truck can be seen in Table 3.6 and the related simulation results are shown in Figures 3.35 and 3.36. As anticipated, with the available motor traction force, less acceleration can be generated for the bicycle model of the small truck. Hence, it is slower for heavier vehicles to reach the reference velocity due to the increased mass and limited traction force.

Table 3.6: Gain Scheduling Parameters for Small Truck

G_{min}^{lin}	G_{max}^{lin}	K_{min}^{lin}
0.05	1.3	1

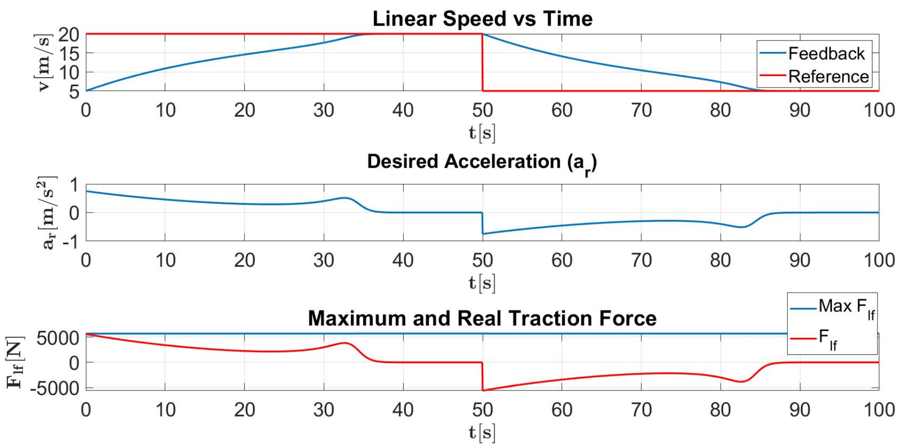

Figure 3.35: Linear Velocity Controller with Gain Schedule of Small Truck for Large Error

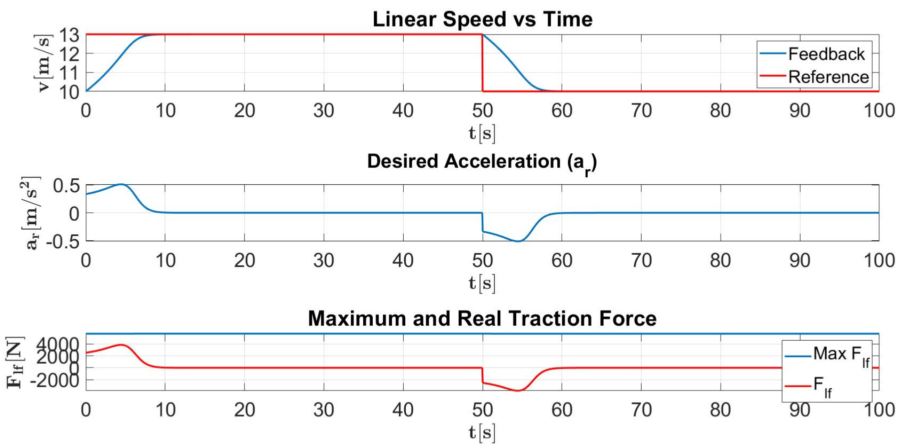

Figure 3.36: Linear Velocity Controller with Gain Schedule of Small Truck for Small Error

3.2.2 Angular Velocity Controller

In Section 3.2.1, a linear velocity controller is developed for the longitudinal vehicle control. In this section, an angular velocity controller is developed in order to manipulate the vehicle's lateral motion. As for the linear velocity controller, a proportional controller is implemented with a gain scheduler since it is more efficient than a simple P controller.

$$\delta = K_p^{ang} e, \tag{3.35}$$

where

$$e = w_{ref} - \dot{\psi}. \tag{3.36}$$

The gain schedule's parameters are defined as in Table 3.7 and the resulting parameters with respect to the error can be seen in Figure 3.37.

Table 3.7: Gain Scheduling Parameters

G_{min}^{ang}	G_{max}^{ang}	K_{min}^{ang}
1	9	10

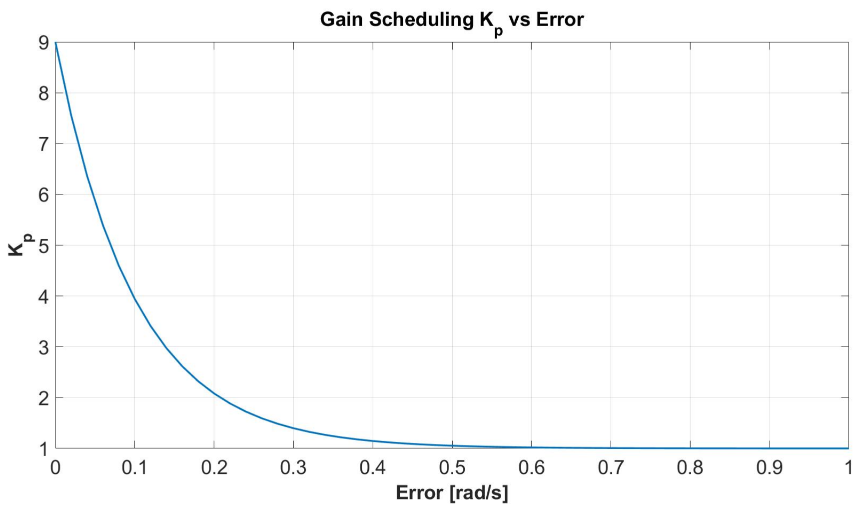

Figure 3.37: Gain Scheduling K_p with respect to error of angular velocity

The angular velocity controller is first tested while the vehicle's speed is constant at 10 m/s. The results can be seen below:

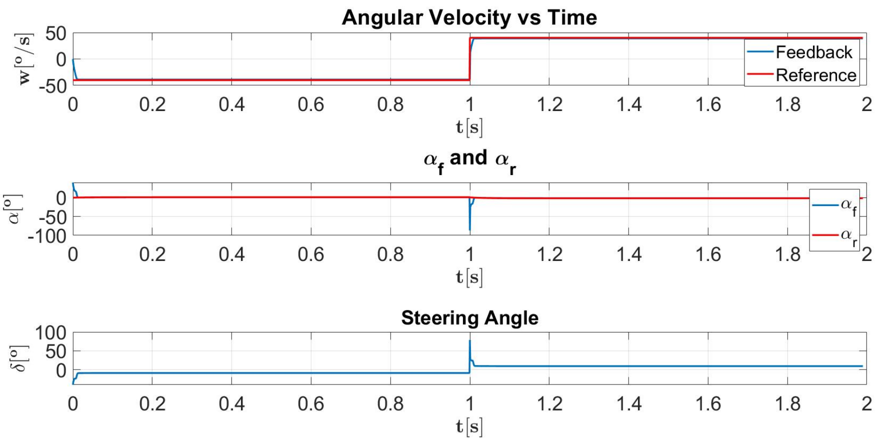

Figure 3.38: Angular Velocity Controller with Gain Schedule when $v = 10(m/s)$

As can be observed in Figure 3.38, when the reference signal changes in an instant there occurs a big spike in the slip angle of the front tire slip. The reason is that the steering angle (δ) changes instantly such that also the error changes instantly. However if a wheel steering controller for steering is implemented for experiments in real vehicles there will not be any issue as spikes in the slip angle of the front tire. The reason is that, in reality, the steering wheel cannot be turned as fast as in Figure 3.38. In order to eliminate the spikes, the controller is changed a bit which can be seen in (3.37) and (3.38). Instead of directly controlling the steering angle, we suggest to control the time derivative of the steering angle.

$$\dot{\delta} = K_p^{ang} * e \tag{3.37}$$

$$\delta = \delta_0 + \int_t \dot{\delta}\, dt \tag{3.38}$$

The results for the new angular velocity controller with the same gain scheduling in 3.7 for K_p^{ang} can be seen below:

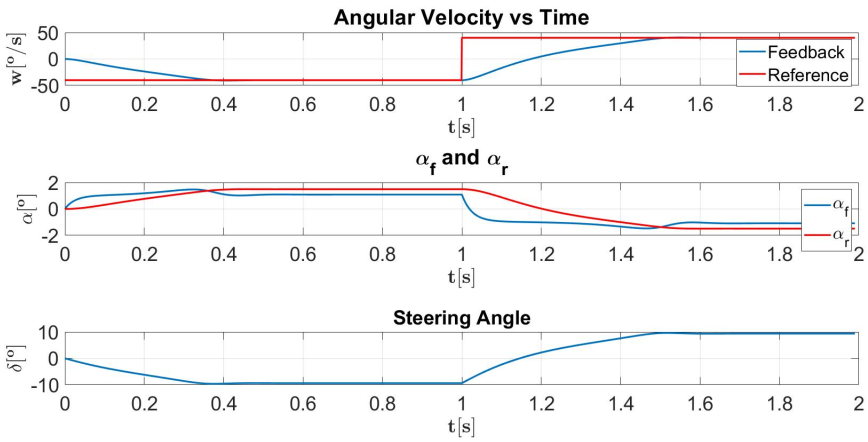

Figure 3.39: Angular Velocity Controller when $v = 10\,$m/s

It also has to be mentioned that the steady-state error between the reference signal and angular velocity of vehicle in figure 3.38 does not appear when using $\dot{\delta}$ as the input signal. This is due to the addition of an integrator in the control loop. However with this controller parameters there is a small overshoot in δ. In the figures below it can be seen that overshoot becomes larger and it becomes oscillating as the linear velocity gets higher.

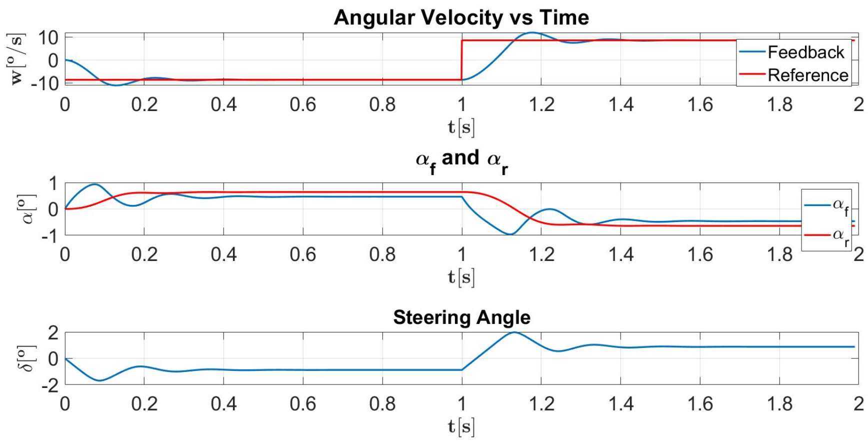

Figure 3.40: Angular Velocity Controller when $v = 20\,$m/s

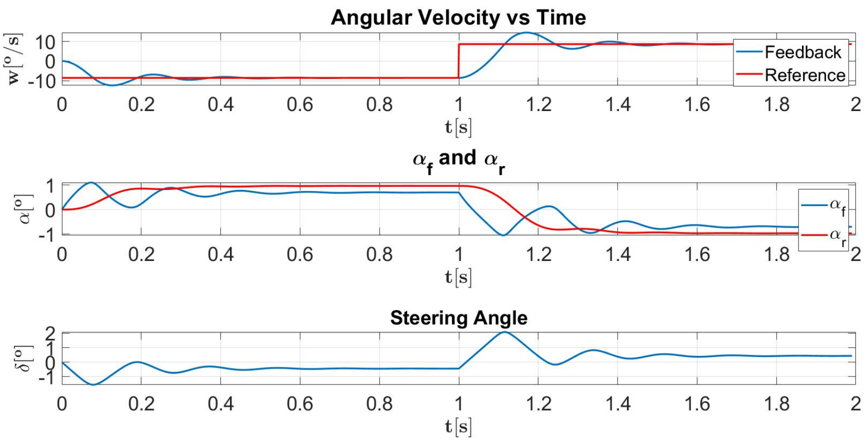

Figure 3.41: Angular Velocity Controller when $v = 30$ m/s

In order to reduce the overshoot and oscillations, the controller should be re-tuned. The re-tuned gain scheduling parameters for the angular velocity controller can be seen in the table below:

Table 3.8: Re-tuned Gain Scheduling Parameters

G^{ang}_{min}	G^{ang}_{max}	K^{ang}_{min}
0.7	3	10

The resulting scheduled gain with respect to error can be seen in the figure below:

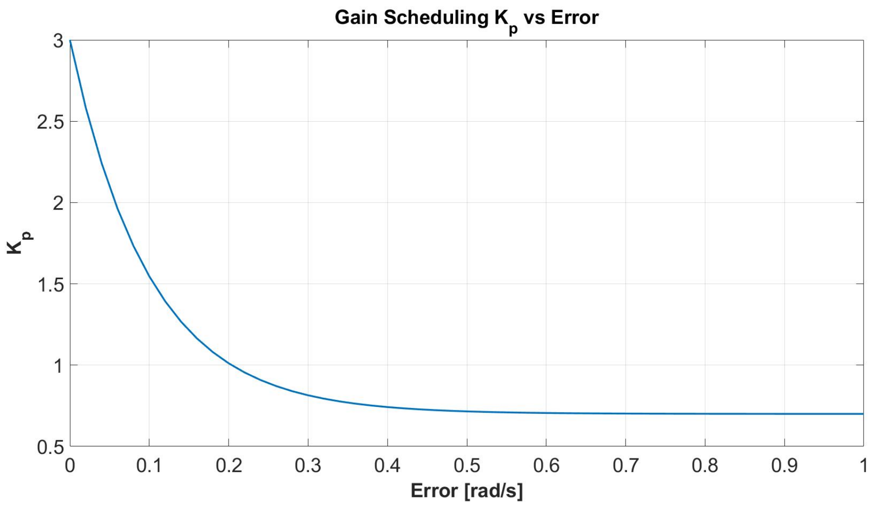

Figure 3.42: Re-tuned scheduled gain K_p^{ang} with respect to error of angular velocity

The results for the re-tuned controller are displayed in Figures 3.43, 3.44 and 3.45. For higher linear velocities of the vehicle, the overshoot cannot be eliminated if enough performance for the nonlinear formation controller is desired. However, re-tuning the angular velocity controller leads to reduced oscillations which would provide a smoother riding experience. In other words, as long as the controller's performance is good enough to provide convergence to the desired position of the vehicle comfortable driving experience should be high priority.

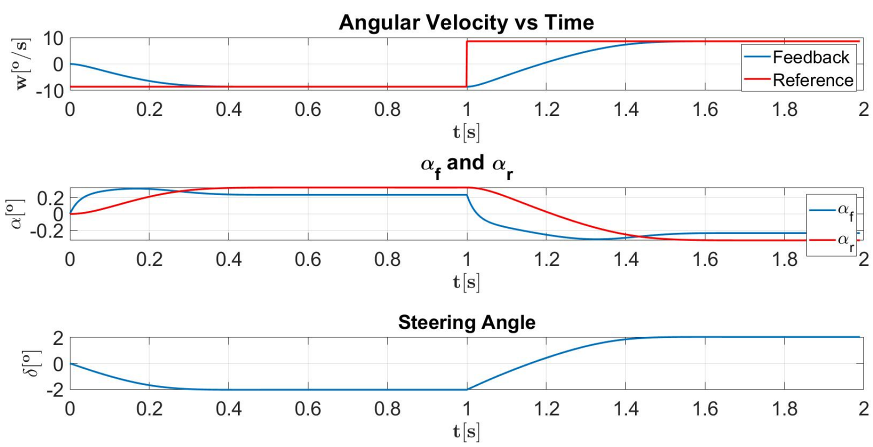

Figure 3.43: Re-tuned Angular Velocity Controller when $v = 10$ m/s

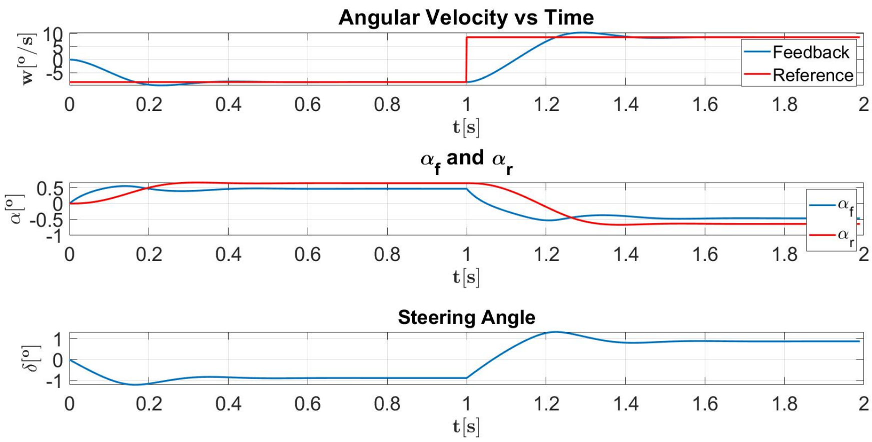

Figure 3.44: Re-tuned Angular Velocity Controller when $v = 20\,\text{m/s}$

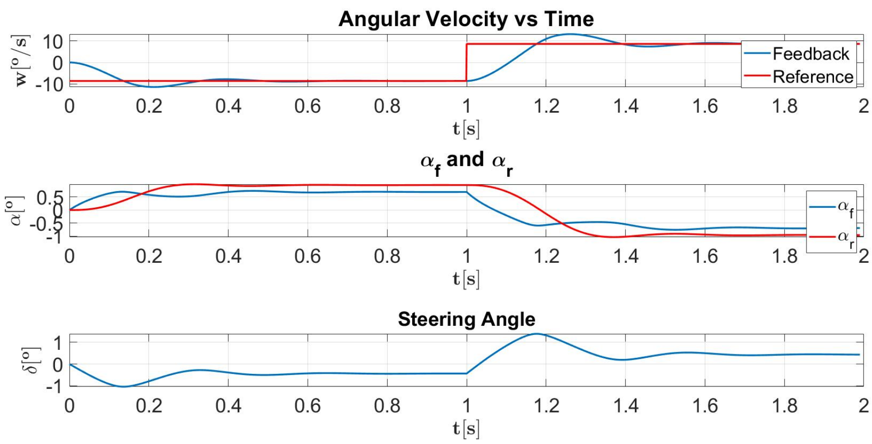

Figure 3.45: Re-tuned Angular Velocity Controller when $v = 30\,\text{m/s}$

3.3 Nonlinear Formation Controller with Dynamic Vehicle Model

A dynamic vehicle model with angular and linear velocity controllers has been obtained in Sec. 3.1. In this section, the nonlinear formation controller based on the Virtual Based controller, which is introduced in 2.3, will be tested with the dynamic model instead of a kinematic model. Block diagram of the system under test can be seen below:

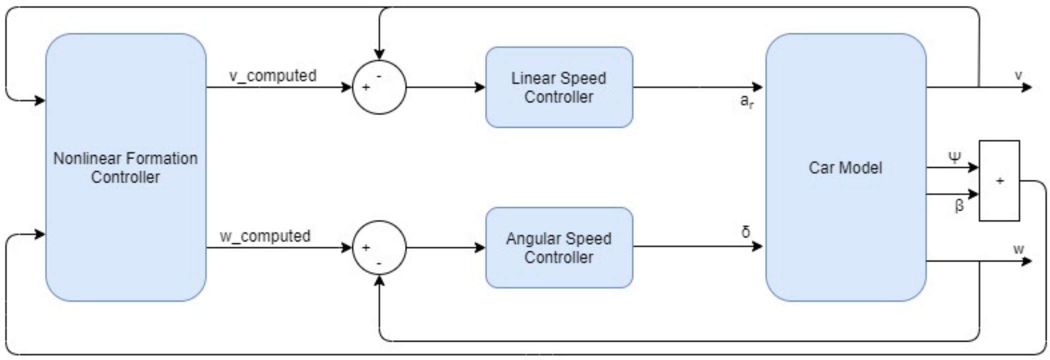

Figure 3.46: Block Diagram of System for Simulation Tests

3.3.1 Assumptions and Limitations

We next state several assumptions for the simulation experiments.

- All vehicles in the fleet are identical. Hence, same vehicle and controller parameters that are covered in Sections 3.1.1 and 3.2 are used for each AV.
- The motor traction force (F_{lf}) is calculated from desired acceleration (a_r) which is explained in Section 3.1.4. In these simulations, motors of the vehicles are assumed to be able to give required motor traction force in instant.
- The motor traction force should be lower than its maximum value which is explained in Section 3.1.4 in order to prevent tires from spinning at any time of the simulation.
- In Section 3.2.2, the control input is explained to be the rate of steering angle (δ). It is assumed that the control input is applied to the wheel exactly.
- The tire slip angle should not exceed $4°$ in order to prevent slipping which is examined in Section 3.1.3.
- The lateral acceleration of the vehicle should not exceed $3.6\,\text{m/s}^2$ in order to achieve at least medium comfort ride which is mentioned in Section 3.1.2.

3.3.2 Simulation Results

Simulations are first run in different cases for a single car. It is assumed that since other vehicles are identical and the same controllers are used they behave similar. At the end, some simulations are run for a fleet of cars.

In this part of the thesis, the tables show initial conditions and desired positions of the vehicles and the control parameters for the nonlinear formation controller, the linear and angular velocity controllers. Figures 3.47, 3.51, 3.55 and 3.59 show linear velocity, angular velocity and lateral acceleration of the virtual leader for different cases. The resulting vehicle positions can be seen in Figures 3.48, 3.52, 3.56, 3.60, 3.63 and 3.65.

For a deeper understanding of cases, results such as error values of position in X and Y axis, slip angle of tires, lateral acceleration and motor traction force of vehicles are given in Figures 3.50, 3.54, 3.58, 3.62, 3.64 and 3.66.

3.3.2.1 Case 1

In this case, only one vehicle is tested with the formation controller. The dynamic vehicle model and kinematic vehicle models are compared with the same formation controller parameters and initial conditions. The linear and angular velocity controller parameters are chosen as described in Section 3.2.1 and 3.2.2. The virtual car's linear and angular velocity is varying during the simulation time as in Figure 3.47. The resulting positions of the kinematic and dynamic models can be seen in Figure 3.48, where both move on very similar paths.

Table 3.9: System Tests Case 1: Desired Positions and Initial Conditions

$x_{des}[m]$	$y_{des}[m]$	$v(0)[m/s]$	$w(0)[^o/s]$	$X(0)[m]$	$Y(0)[m]$
4	10	20	0	-7	20

Table 3.10: System Tests Case 1: Controller Parameters

k	k_θ	G_{min}^{lin}	G_{max}^{lin}	K_{min}^{lin}	G_{min}^{ang}	G_{max}^{ang}	K_{min}^{ang}
1	3	0.27	8	1	0.7	3	10

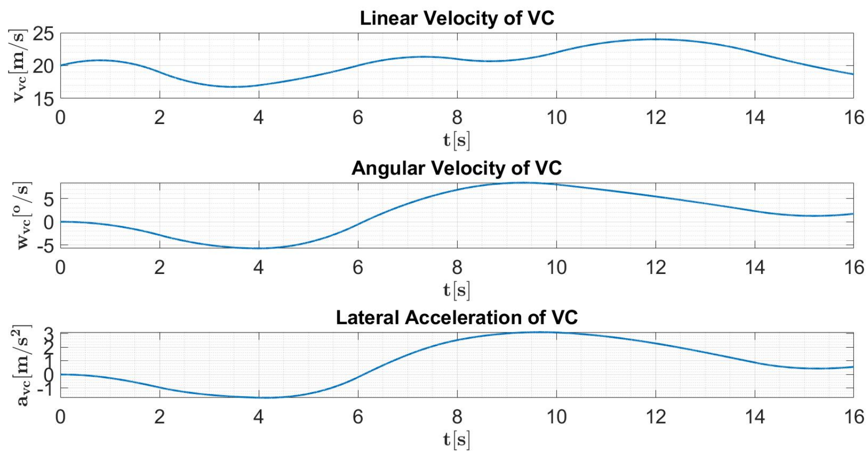

Figure 3.47: Case 1: Linear Velocity, Angular Velocity and Lateral Acceleration of Virtual Car

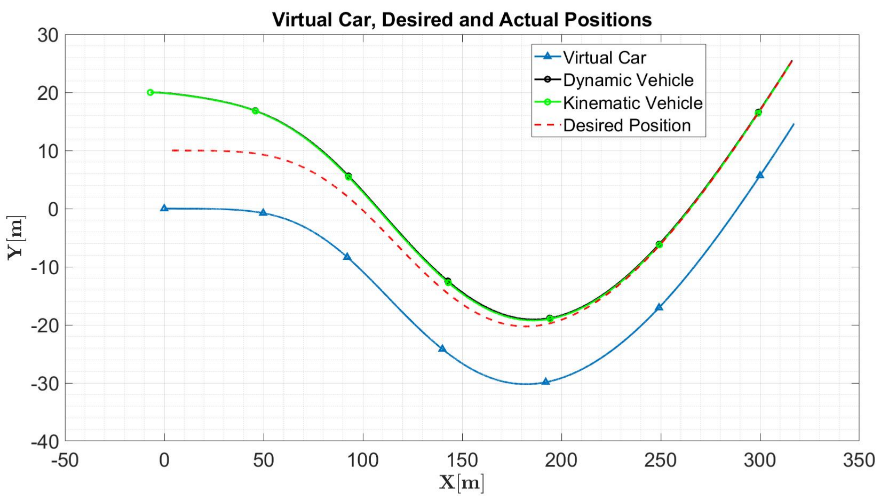

Figure 3.48: Case 1: Positions of Vehicles in Global Coordinates Frame

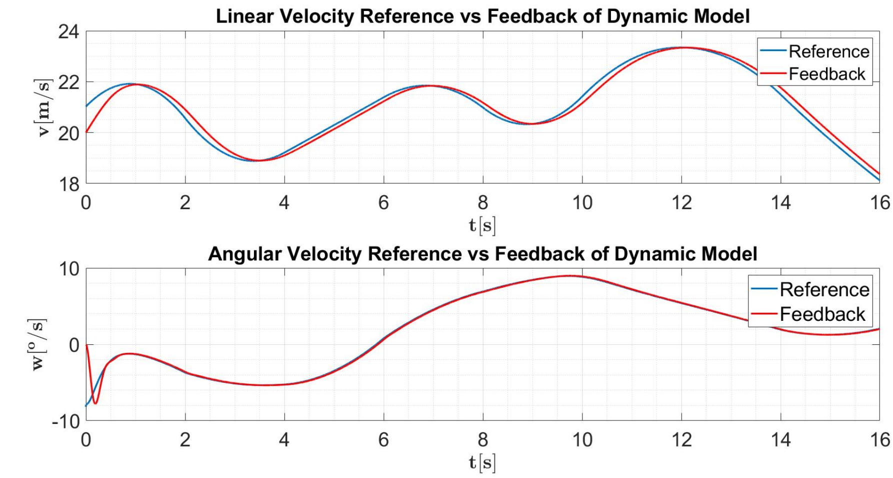

Figure 3.49: Case 1: Angular and Linear Reference and Velocity

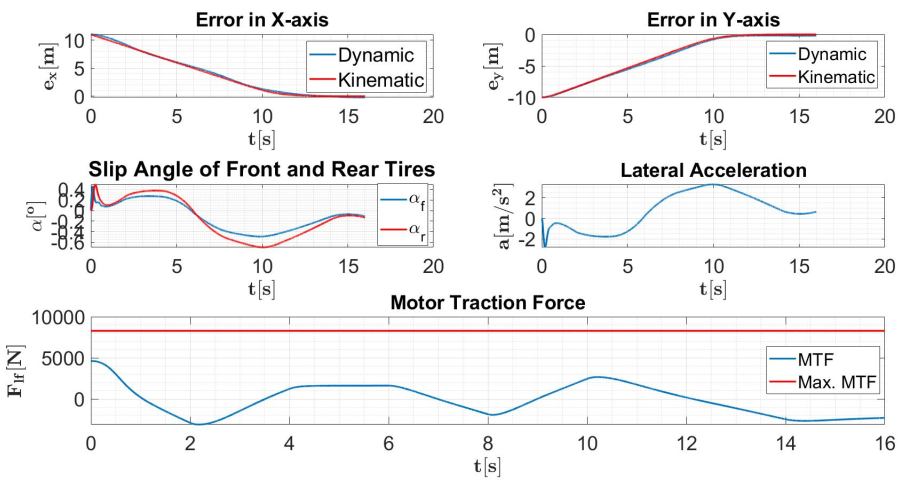

Figure 3.50: Case 1: Errors in X and Y Directions, Slip Angle, Lateral Acceleration and Motor Traction Force

3.3.2.2 Case 2

This case has the same inputs, initial conditions and parameters except for the linear velocity controller which can be seen in Table 3.12. The linear velocity controller parameters are chosen such that the controller perform poorly, which can be seen in Figure 3.53. The dynamic vehicle model is not able to track the desired position in Figure 3.52 with a poor linear velocity controller.

Table 3.11: System Tests Case 2: Desired Positions and Initial Conditions

$x_{des}[m]$	$y_{des}[m]$	$v(0)[m/s]$	$w(0)[^o/s]$	$X(0)[m]$	$Y(0)[m]$
4	10	20	0	-7	20

Table 3.12: System Tests Case 2: Controller Parameters

k	k_θ	G^{lin}_{min}	G^{lin}_{max}	K^{lin}_{min}	G^{ang}_{min}	G^{ang}_{max}	K^{ang}_{min}
1	3	0.2	3	1	0.7	3	10

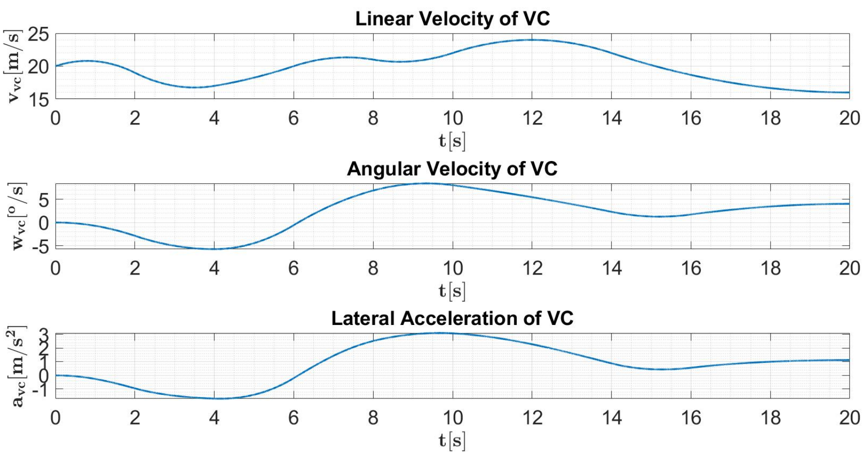

Figure 3.51: Case 2: Linear Velocity, Angular Velocity and Lateral Acceleration of Virtual Car

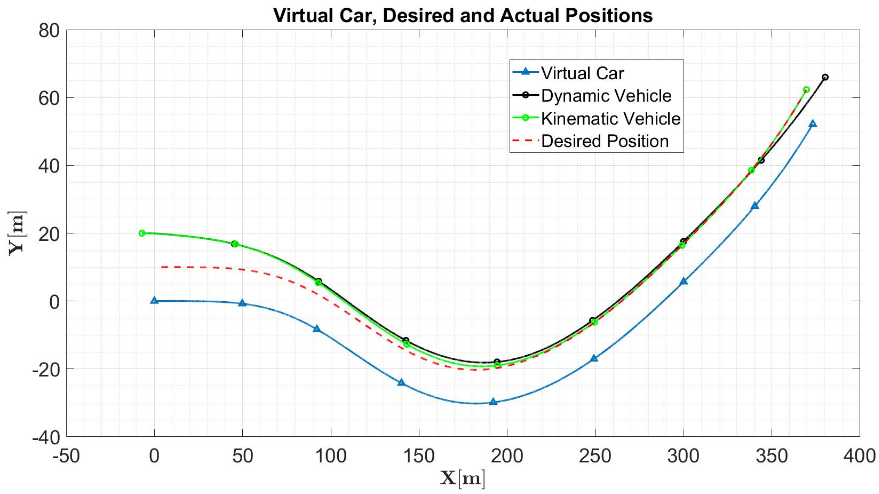

Figure 3.52: Case 2: Positions of Vehicles in Global Coordinates Frame

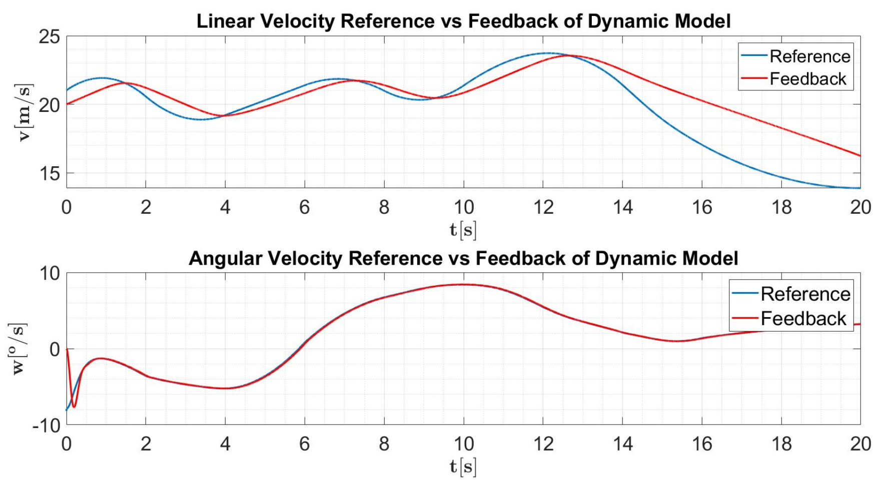

Figure 3.53: Case 2: Angular and Linear Reference and Velocity

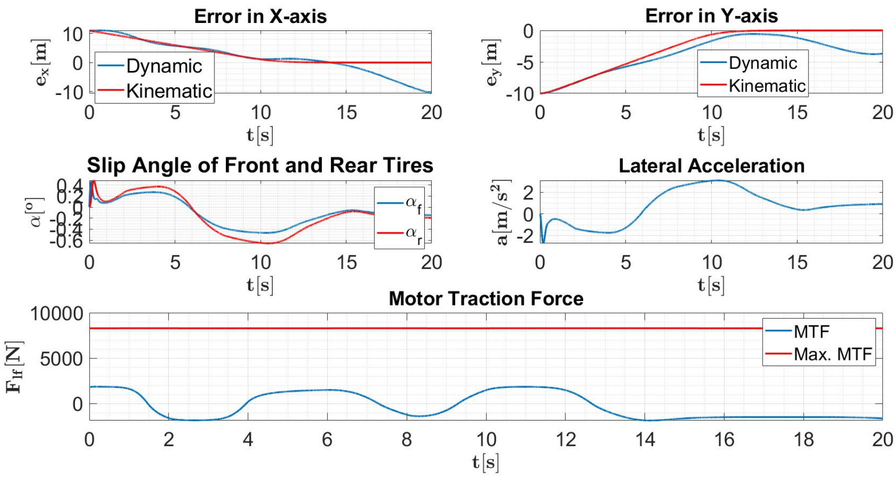

Figure 3.54: Case 2: Errors in X and Y Directions, Slip Angle, Lateral Acceleration and Motor Traction Force

3.3.2.3 Case 3

In the first and second case, the linear velocity of virtual car and vehicle is the same at the beginning of the simulation ($v(0) = v_{vc}(0) = 20$ m/s). In this case, it will be examined how a difference in the vehicle's and virtual vehicle's initial linear speed affects the formation controller's performance. For the same parameters as in Tables 3.13, 3.14, the inputs in Figures 3.55 and 3.59 are supplied for two different simulations, where the initial linear speed is $v(0) = 10$ m/s and $v(0) = 15$ m/s, respectively. The main result in Figure 3.60 is that when the initial linear speed of the vehicle is $15m/s$, the vehicle can still track the desired position even though it is slower to settle than in Figure 3.48. On the other hand, as the difference between the initial velocity of the virtual vehicle and the vehicle gets bigger, the vehicle more slowly settles on the desired position, which can be seen in Figure 3.56. Furthermore, when comparing the errors between the described cases with different initial velocity values in Figures 3.58 and 3.62, it can be seen that the errors in X-axis and Y-axis converge to zero for $v(0) = 15$ m/s and $v(0) = 10$ m/s. Therefore, difference between initial linear velocity values of the virtual car and vehicles in the fleet should not be too large when the formation controller starts in order to get high performance from the formation controller.

Table 3.13: System Tests Case 3: Desired Positions and Initial Conditions

$x_{des}[m]$	$y_{des}[m]$	$v(0)[m/s]$	$w(0)[^o/s]$	$X(0)[m]$	$Y(0)[m]$
4	10	$10/15$	0	-7	20

Table 3.14: System Tests Case 3: Controller Parameters

k	k_θ	G_{min}^{lin}	G_{max}^{lin}	K_{min}^{lin}	G_{min}^{ang}	G_{max}^{ang}	K_{min}^{ang}
1	3	0.27	8	1	0.7	3	10

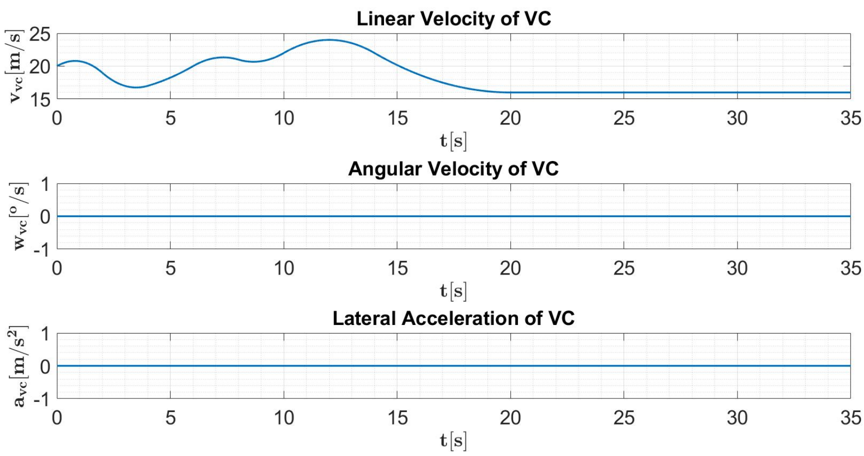

Figure 3.55: Case 3: Linear Velocity, Angular Velocity and Lateral Acceleration of Virtual Car for $v(0) = 10\,\text{m/s}$

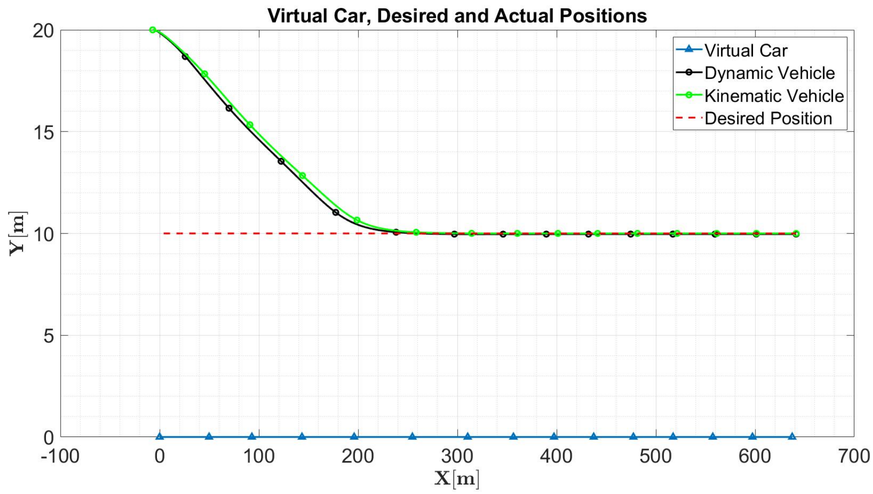

Figure 3.56: Case 3: Positions of Vehicles in Global Coordinates Frame for $v(0) = 10\,\text{m/s}$

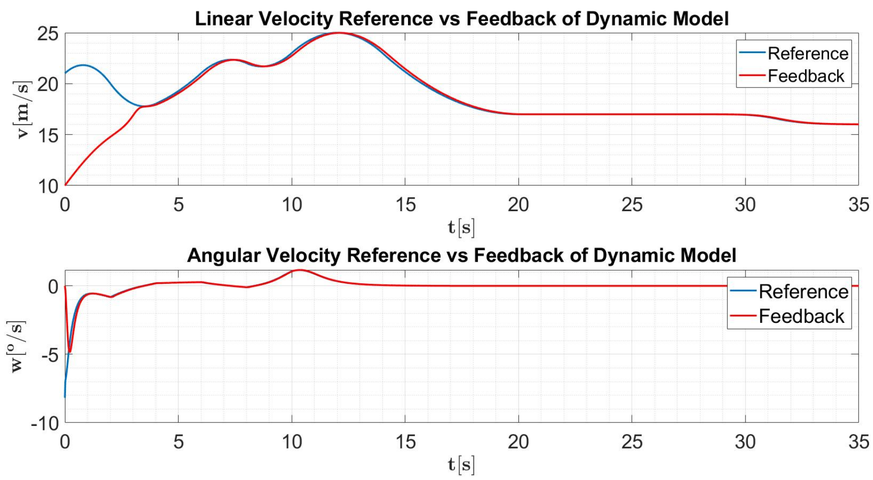

Figure 3.57: Case 3: Angular and Linear Reference and Velocity for $v(0) = 10\,\text{m/s}$

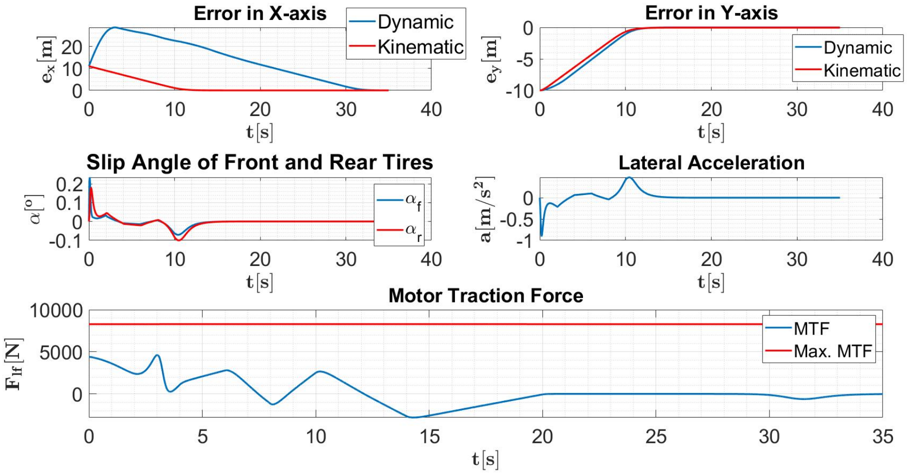

Figure 3.58: Case 3: Errors in X and Y Directions, Slip Angle, Lateral Acceleration and Motor Traction Force for $v(0) = 10\,\mathrm{m/s}$

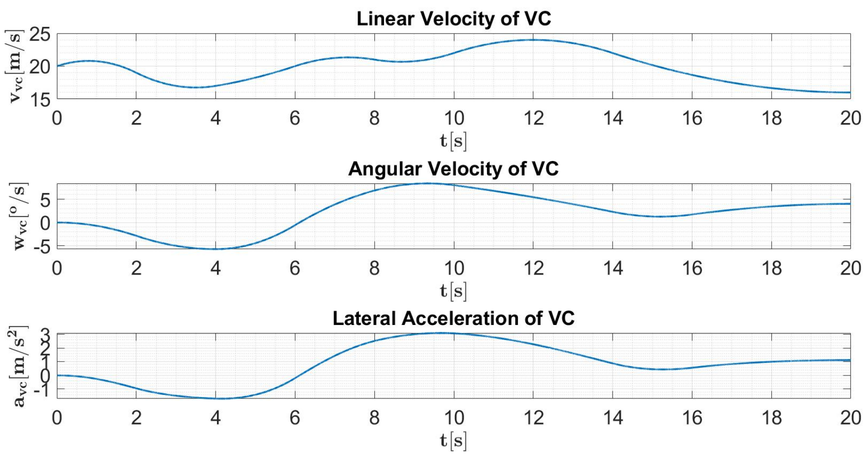

Figure 3.59: Case 3: Linear Velocity, Angular Velocity and Lateral Acceleration of Virtual Car for $v(0) = 15\,\mathrm{m/s}$

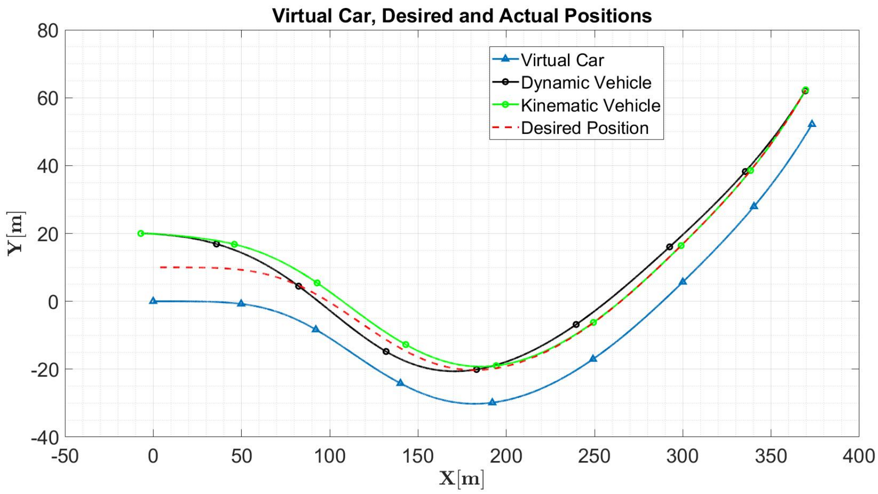

Figure 3.60: Case 3: Positions of Vehicles in Global Coordinates Frame for $v(0) = 15\,\text{m/s}$

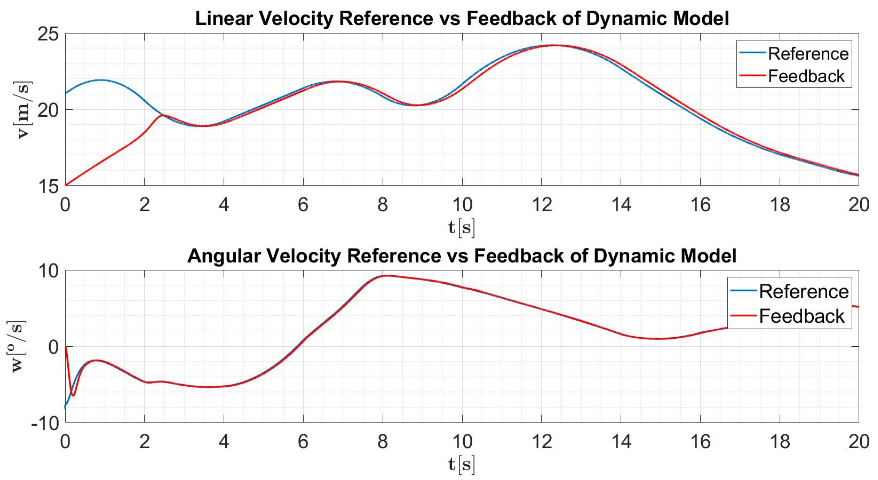

Figure 3.61: Case 3: Angular and Linear Reference and Velocity for $v(0) = 15\,\text{m/s}$

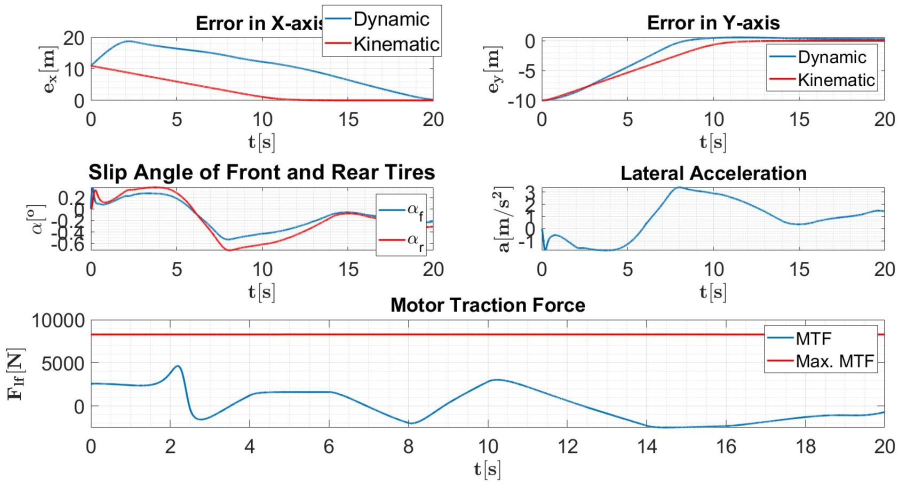

Figure 3.62: Case 3: Errors in X and Y Directions, Slip Angle, Lateral Acceleration and Motor Traction Force for $v(0) = 15\,\mathrm{m/s}$

3.3.2.4 Case 4

In this case, three different vehicles with the same desired positions start from different positions, where the virtual vehicle is moving with no angular velocity and a constant angular velocity. When the errors are compared in Figures 3.64 and 3.66, it can be seen that the vehicles move to the desired position with respect to the virtual vehicle's current position with a constant rate in both cases. Therefore, it can be concluded that the settling time is inversely proportional to the error between the vehicle's current position and desired position.

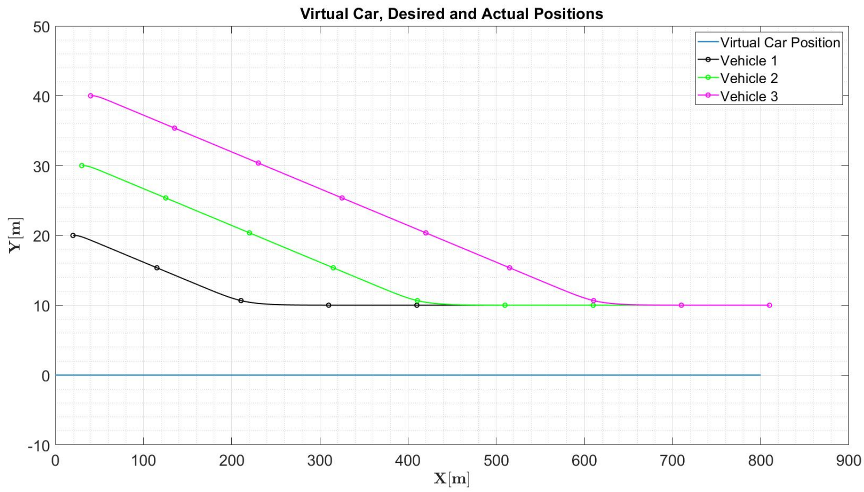

Figure 3.63: Case 4: Positions of Vehicles in Global Coordinates Frame without Angular Velocity of Virtual Vehicle

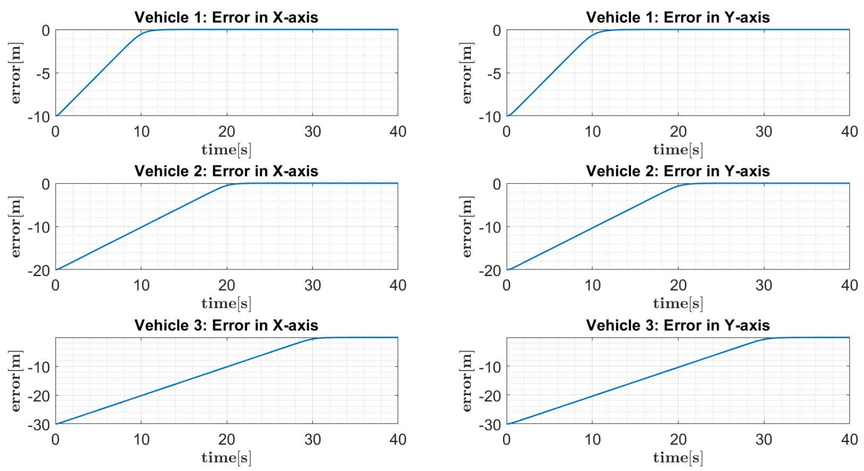

Figure 3.64: Case 4: Errors in x and y Directions without Angular Velocity of Virtual Vehicle

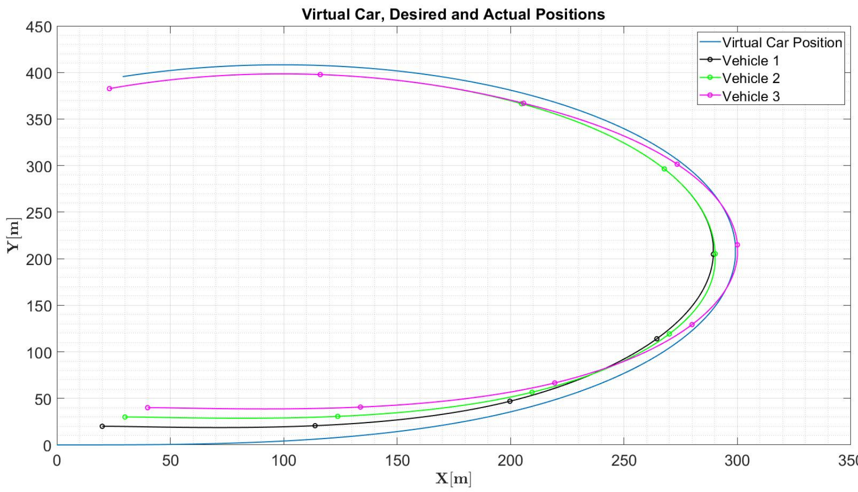

Figure 3.65: Case 4: Positions of Vehicles in Global Coordinates Frame with Constant Angular Velocity of Virtual Vehicle

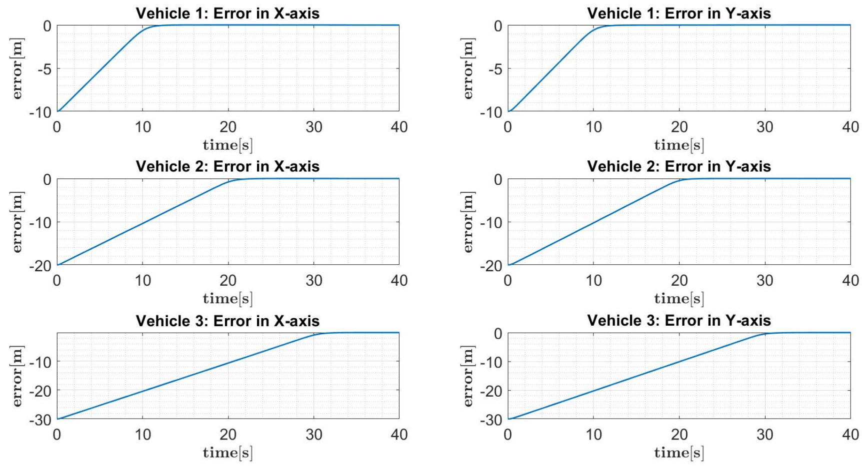

Figure 3.66: Case 4: Errors in x and y Directions with Constant Angular Velocity of Virtual Vehicle

CHAPTER 4

CONCLUSION

The development of autonomous vehicles (AVs) is a state-of-art study subject for the industry and academic literature. As a special topic, formation control becomes an important subject in order to move autonomous vehicles in harmony. In the case of AVs being used frequently in the upcoming decades, formation control theory would help to overcome traffic issues or to develop transportation to the next level.

In this thesis study, different methods which are leader-follower, behavior based and virtual based approaches in literature to achieve formation control are summarized. Each method's advantages or disadvantages are listed. The formation controller used in this thesis is developed using an existing virtual vehicle based method from the literature. This method designs a nonlinear control algorithm based on a kinematic vehicle model. The nonlinear formation controller computes the path for vehicles to be able to track a pre-defined position with respect to the virtual vehicle traveling on a route. In previous work, it was assumed that the kinematic model of the vehicles can directly realize the control inputs from the formation controller, which are the longitudinal and angular velocity of the vehicle. Nevertheless, it has to be pointed out that, in practice, the actual vehicle dynamics have to be considered, where both the longitudinal and the angular velocity are states of the vehicle and hence cannot be directly controlled.

Accordingly, in this thesis, the nonlinear formation control algorithm is applied to a more realistic model. This realistic model is based on the dynamic bicycle car model which is a simple dynamic vehicle model used in literature. As the tire model, Pajecka's tire model is implemented. As the slip angles of the tires are supposed to be small in the relevant driving scenarios, a linearized tire model is derived from the nonlinear model. Furthermore, additional practical constraints are considered for the vehicle model. First, it is assumed that the motor traction force applied is limited depending on the vehicle characteristics and road adhesion. Second, it is assumed that the steering angle cannot be changed instantaneously such that the control input for steering is the time derivative of the steering angle. Using these assumptions, the main contribution of the thesis is the development of a control structure that uses the longitudinal and angular velocity provided by the nonlinear formation controller as reference signals and computes suitable acceleration and steering inputs for the dynamic bicycle model in order to track these reference signals. To this end, two controllers are tuned and implemented using gain scheduling for proportional constants. Furthermore a simulation study is carried out. In these simulations, different cases are tested with one vehicle in the fleet assuming all vehicles will behave similarly. In the first case, the dynamic vehicle model is tested where linear and angular velocity of the virtual vehicle varies in time and it is concluded that the dynamic model behaves very similarly to the kinematic model. In the second case, it is shown that poor tuning of the controller parameters negatively effects the convergence to the desired trajectory. Specifically, when the velocity controller's parameters are changed such that vehicle's speed can not follow the reference signal supplied from the formation controller, the dynamic model can not follow the path of the kinematic model and the error in both the x and y direction does not converge to zero. Hence, it can be concluded that the performance of the velocity controller is highly important for the formation controller to work properly. In the first two cases, the vehicle's linear speed is the same as the virtual leader's. In the third case, it is tested whether the vehicle can follow its path to the desired position or not. As the initial speed of the vehicle gets further away from the virtual leader's, it becomes harder for the vehicle to reach its desired position. In the last case, the vehicle is tested with different initial positions where its desired position is same. As the vehicle's initial positions gets further away from the desired position, its settling time to reach the desired position rises proportionally since the rate of change of the errors in x and y direction is constant.

In conclusion, the nonlinear formation controller can be used for nonholonomic dynamic bicycle car model with well performing velocity controllers which is more realistic than the kinematic model used to design the formation controller. In the future, the model can be extended implementing motor and steering models to get even more realistic results. Furthermore, simulations can be done for different types of vehicles such as trucks, nonholonomic robots on different types of roads such as rainy or icy asphalt. The formation controller can further be tested on real nonholonomic robots implemented with velocity controllers and compared to the simulation results.

REFERENCES

[1] A. H. M. A. KAHIYA, “Optimal control problems for safe and efficient lane changes of self-driving vehicles,” *Dep. of Electric and Communication Engineering., Çankaya Üniv., Ankara*, 2017.

[2] A. Rucco, G. Notarstefano, and J. Hauser, “Optimal control based dynamics exploration of a rigid car with longitudinal load transfer,” *IEEE Transactions on Control Systems Technology*, vol. 22, no. 3, pp. 1070–1077, 2013.

[3] L. Chen and M. Baoli, “A nonlinear formation control of wheeled mobile robots with virtual structure approach,” in *2015 34th Chinese Control Conference (CCC)*, pp. 1080–1085, IEEE, 2015.

[4] S. S. Shadrin and A. A. Ivanova, “Analytical review of standard sae j3016 «taxonomy and definitions for terms related to driving automation systems for on-road motor vehicles» with latest updates,” *Avtomobil’. Doroga. Infrastruktura.*, no. 3 (21), p. 10, 2019.

[5] E. Yurtsever, J. Lambert, A. Carballo, and K. Takeda, “A survey of autonomous driving: Common practices and emerging technologies,” *IEEE access*, vol. 8, pp. 58443–58469, 2020.

[6] M. N. Ahangar, Q. Z. Ahmed, F. A. Khan, and M. Hafeez, “A survey of autonomous vehicles: Enabling communication technologies and challenges,” *Sensors*, vol. 21, no. 3, p. 706, 2021.

[7] A. Alsalman, L. N. Assi, S. Ghotbi, S. Ghahari, and A. Shubbar, “Users, planners, and governments perspectives: A public survey on autonomous vehicles future advancements,” *Transportation Engineering*, vol. 3, p. 100044, 2021.

[8] J. Hu, P. Bhowmick, F. Arvin, A. Lanzon, and B. Lennox, “Cooperative control of heterogeneous connected vehicle platoons: An adaptive leader-following

approach," *IEEE Robotics and Automation Letters*, vol. 5, no. 2, pp. 977–984, 2020.

[9] T. Sturm, C. Krupitzer, M. Segata, and C. Becker, "A taxonomy of optimization factors for platooning," *IEEE Transactions on Intelligent Transportation Systems*, 2020.

[10] S. Thormann, A. Schirrer, and S. Jakubek, "Safe and efficient cooperative platooning," *IEEE Transactions on Intelligent Transportation Systems*, 2020.

[11] D. Rojas-Rueda, M. J. Nieuwenhuijsen, H. Khreis, and H. Frumkin, "Autonomous vehicles and public health," *Annual review of public health*, vol. 41, pp. 329–345, 2020.

[12] P. Kavathekar and Y. Chen, "Vehicle platooning: A brief survey and categorization," in *International Design Engineering Technical Conferences and Computers and Information in Engineering Conference*, vol. 54808, pp. 829–845, 2011.

[13] P. Shi and B. Yan, "A survey on intelligent control for multiagent systems," *IEEE Transactions on Systems, Man, and Cybernetics: Systems*, vol. 51, no. 1, pp. 161–175, 2020.

[14] A. Soni and H. Hu, "Formation control for a fleet of autonomous ground vehicles: A survey," *Robotics*, vol. 7, no. 4, p. 67, 2018.

[15] H. Goldstein, C. Poole, and J. Safko, "Classical mechanics," 2002.

[16] B. Torby, "Energy methods," *Advanced Dynamics for Engineers. HRW Series in Mechanical Engineering. United States of America: CBS College Publishing*, 1984.

[17] H. Hertz and J. T. Walley, *The principles of mechanics presented in a new form*. Macmillian and Company, Limited, 1899.

[18] B. Triggs, "Motion planning for nonholonomic vehicles: An introduction," 1993.

[19] J. Chunyu, Z. Qu, E. Pollak, and M. Falash, "A new multi-objective control design for autonomous vehicles," in *Optimization and Cooperative Control Strategies*, pp. 81–102, Springer, 2009.

[20] H. R. Maei and R. S. Sutton, "Gq (λ): A general gradient algorithm for temporal-difference prediction learning with eligibility traces," in *Proceedings of the third conference on artificial general intelligence*, vol. 1, pp. 91–96, Citeseer, 2010.

[21] M. Knopp, C. Aykın, J. Feldmaier, and H. Shen, "Formation control using gq (λ) reinforcement learning," in *2017 26th IEEE International Symposium on Robot and Human Interactive Communication (RO-MAN)*, pp. 1043–1048, IEEE, 2017.

[22] R. Li, L. Zhang, L. Han, and J. Wang, "Multiple vehicle formation control based on robust adaptive control algorithm," *IEEE Intelligent Transportation Systems Magazine*, vol. 9, no. 2, pp. 41–51, 2017.

[23] Z. Peng, S. Yang, G. Wen, A. Rahmani, and Y. Yu, "Adaptive distributed formation control for multiple nonholonomic wheeled mobile robots," *Neurocomputing*, vol. 173, pp. 1485–1494, 2016.

[24] F. Michaud and M. Nicolescu, "Behavior-based systems," in *Springer handbook of robotics*, pp. 307–328, Springer, 2016.

[25] J. R. Lawton, R. W. Beard, and B. J. Young, "A decentralized approach to formation maneuvers," *IEEE transactions on robotics and automation*, vol. 19, no. 6, pp. 933–941, 2003.

[26] Y. Tang and L. E. Parker, "Towards schema-based, constructivist robot learning: Validating an evolutionary search algorithm for schema chunking," in *2008 IEEE International Conference on Robotics and Automation*, pp. 2837–2844, IEEE, 2008.

[27] T. Balch and R. C. Arkin, "Behavior-based formation control for multirobot teams," *IEEE transactions on robotics and automation*, vol. 14, no. 6, pp. 926–939, 1998.

[28] R. Kuppan Chetty, M. Singaperumal, and T. Nagarajan, "Behavior based multi robot formations with active obstacle avoidance based on switching control strategy," in *Advanced Materials Research*, vol. 433, pp. 6630–6635, Trans Tech Publ, 2012.

[29] Y. Zhang, G. Song, G. Qiao, J. Zhang, and J. Peng, "Consensus and obstacle avoidance for multi-robot systems with fixed and switching topologies," in *2014 IEEE International Conference on Robotics and Biomimetics (ROBIO 2014)*, pp. 1213–1218, IEEE, 2014.

[30] E. Semsar-Kazerooni, K. Elferink, J. Ploeg, and H. Nijmeijer, "Multi-objective platoon maneuvering using artificial potential fields," *IFAC-PapersOnLine*, vol. 50, no. 1, pp. 15006–15011, 2017.

[31] W. Ren and R. W. Beard, "Decentralized scheme for spacecraft formation flying via the virtual structure approach," *Journal of Guidance, Control, and Dynamics*, vol. 27, no. 1, pp. 73–82, 2004.

[32] K.-H. Tan and M. A. Lewis, "Virtual structures for high-precision cooperative mobile robotic control," in *Proceedings of IEEE/RSJ International Conference on Intelligent Robots and Systems. IROS'96*, vol. 1, pp. 132–139, IEEE, 1996.

[33] X. Qian, A. De La Fortelle, and F. Moutarde, "A hierarchical model predictive control framework for on-road formation control of autonomous vehicles," in *2016 IEEE Intelligent Vehicles Symposium (IV)*, pp. 376–381, IEEE, 2016.

[34] C. B. Low, "Adaptable virtual structure formation tracking control design for nonholonomic tracked mobile robots, with experiments," in *2015 IEEE 18th International Conference on Intelligent Transportation Systems*, pp. 1868–1875, IEEE, 2015.

[35] A. Essghaier, L. Beji, M. A. El Kamel, A. Abichou, and J. Lerbet, "Co-leaders and a flexible virtual structure based formation motion control," *International journal of vehicle autonomous systems*, vol. 9, no. 1-2, pp. 108–125, 2011.

[36] R. Rajamani, *Vehicle dynamics and control*. Springer Science & Business Media, 2011.

[37] W. Cheng, "Study on the evaluation method of highway alignment comfortableness [ms thesis]," *Hebei University of Technology, Tianjin, China*, 2007.

[38] J. Xu, K. Yang, Y. Shao, and G. Lu, "An experimental study on lateral acceleration of cars in different environments in sichuan, southwest china," *Discrete Dynamics in nature and Society*, vol. 2015, 2015.

[39] H. Pacejka, *Tire and vehicle dynamics*. Elsevier, 2005.

[40] H. Pacejka and I. Besselink, “Magic formula tyre model with transient properties,” *Vehicle system dynamics*, vol. 27, no. S1, pp. 234–249, 1997.

[41] R. Attia, R. Orjuela, and M. Basset, “Coupled longitudinal and lateral control strategy improving lateral stability for autonomous vehicle,” in *2012 American Control Conference (ACC)*, pp. 6509–6514, IEEE, 2012.

[42] G. Mastinu and M. Plöchl, *Road and off-road vehicle system dynamics handbook*. CRC press, 2014.

[43] F. L. Mannering and S. S. Washburn, *Principles of highway engineering and traffic analysis*. John Wiley & Sons, 2020.

[44] Z. Wu, Y. Liu, and G. Pan, “A smart car control model for brake comfort based on car following,” *IEEE transactions on intelligent transportation systems*, vol. 10, no. 1, pp. 42–46, 2008.

[45] E. Dovgan, T. Tušar, M. Javorski, and B. Filipič, “Discovering comfortable driving strategies using simulation-based multiobjective optimization,” *Informatica*, vol. 36, no. 3, 2012.

[46] A. K. Nandi, D. Chakraborty, and W. Vaz, “Design of a comfortable optimal driving strategy for electric vehicles using multi-objective optimization,” *Journal of Power Sources*, vol. 283, pp. 1–18, 2015.

[47] J. P. Wideberg, “Simplified method for evaluation of the lateral dynamic behaviour of a heavy vehicle,” *International Journal of Heavy Vehicle Systems*, vol. 11, no. 2, pp. 195–207, 2004.